

AutoKnots: Adaptive Knot Allocation for Spline Interpolation

Sandro D. P. Vienti,^a Fernando de Simoni,^b Mariana Penna-Lima,^{c,a} Eduardo J. Barroso,^{d,a}

^aDepartamento de Física, Universidade Estadual de Londrina,
Rod. Celso Garcia Cid, Km 380, 86057-970, Londrina, Paraná, Brazil,

^bDepartamento de Ciências da Natureza, Universidade Federal Fluminense,
Rua Recife, Lotes, 1-7, Jardim Bela Vista, Rio das Ostras - RJ, 28895-532, Brazil,

^cCentro Internacional de Física, Instituto de Física, Universidade de Brasília,
70910-900, Brasília, DF, Brasil,

^dLAPP, Université de Savoie, CNRS/IN2P3, Annecy-Le-Vieux, France

E-mail: vienti@uel.br, fsimoni@id.uff.br, pennalima@unb.br,
barroso@lapp.in2p3.fr

Abstract. In astrophysical and cosmological analyses, the increasing quality and volume of astronomical data demand efficient and precise computational tools. Interpolation methods, particularly spline-based approaches, play a critical role in this context. This work introduces a novel adaptive algorithm for automatic knots (AutoKnots) allocation in spline interpolation, designed to meet user-defined precision requirements. Unlike traditional methods that rely on manually configured knot distributions with numerous parameters, the proposed technique automatically determines the optimal number and placement of knots based on interpolation error criteria. This simplifies configuration, often requiring only a single parameter. The algorithm progressively improves the interpolation by adaptively sampling the function-to-be-approximated, $f(x)$, in regions where the interpolation error exceeds the desired threshold. All function evaluations contribute directly to the final approximation, ensuring efficiency. While each resampling step involves recomputing the interpolation table, this process is highly optimized and usually computationally negligible compared to the cost of evaluating $f(x)$. However, for inherently fast functions, interpolation may not offer significant benefits. We show the algorithm's efficacy through a series of precision tests on different functions. However, the study underscores the necessity for caution when dealing with certain function types, notably those featuring plateaus. To address this challenge, a heuristic enhancement is incorporated, improving accuracy in flat regions. Originally developed in 2007 and integrated into the Numerical Cosmology library (NumCosmo), this algorithm has been extensively used and tested over the years. NumCosmo includes a comprehensive set of unit tests that rigorously evaluate the algorithm both directly and indirectly, underscoring its robustness and reliability. As a practical application, we compute the surface mass density $\Sigma(R)$ and the average surface mass density $\bar{\Sigma}(< R)$ for Navarro-Frenk-White and Hernquist halo density profiles, which provide analytical benchmarks. The adaptive, slim algorithm is implemented in NumCosmo, offering a mature and user-friendly tool for interpolation challenges in computational astrophysics and cosmology.

¹Corresponding author.

Contents

1	Introduction	1
2	The adaptive method	3
2.1	Definitions	3
2.2	Adaptive Algorithm	4
2.3	Tolerance and Scale Parameters	5
2.4	Error Analysis	6
2.5	The <code>refine</code> option	8
3	Testing AutoKnots	9
3.1	The Adaptive Method Applied to a Smooth Function	10
3.2	Testing the <code>refine</code> option	12
3.3	Scale Parameter	13
3.4	Statistical Performance Evaluation	16
3.4.1	Smooth Function $P_6(x)$	20
3.4.2	Highly Variable Function $C_s(x)$	21
3.4.3	Intermediate Function $E_s(x)$	22
3.4.4	Refinement Analysis	24
4	Applications in Cosmology	24
5	Conclusions and Final Remarks	26
A	Algorithmic Implementation	33
A.1	Cubic Spline Interpolation	33
A.1.1	Formulating the Linear System for Spline Coefficients	34
A.2	Adaptive Spline Function	37

1 Introduction

Cosmology and astrophysics are entering a high-precision era driven by the large influx of high-quality data from large-scale surveys. These ongoing and near-future galaxy surveys, such as the Dark Energy Spectroscopic Instrument (DESI) [1], the Javalambre Physics of the Accelerating Universe Astrophysical Survey (J-PAS) [2], Euclid [3], the Rubin Observatory Legacy Survey of Space and Time (LSST) [4] and the Nancy Grace Roman Telescope [5], encompass a broad range of observational data enabling the exploration of fundamental questions such as the nature of dark energy and dark matter.

However, as the precision of cosmological and astrophysical analyses improves, the nature of the challenges shifts. Statistical errors, once a primary concern, are now becoming less significant than systematic ones. Furthermore, advancements in our understanding of various dynamic astrophysical and cosmological phenomena make their numerical modeling increasingly detailed and complex. The Hubble tension exemplifies this current landscape, as it has been the focus of extensive investigation, involving the exploration of modeling approaches, systematic errors, and even the consideration of new physics [6–8].

A third, but no less important, source of error is the numerical error. The relevance of well-tested and optimized computational codes cannot be overstated. The complexity of modern cosmological and astrophysical models demands that the tools used for analysis be rigorously validated to ensure their accuracy. Any flaws in these codes can introduce numerical errors, which, if left unchecked, could lead to spurious results that undermine the integrity of the research. Therefore, the development and maintenance of reliable software are critical to advancing our understanding of the universe. An efficient practice to overcome this problem is the distribution of independent and open-source programming libraries. We can mention some good examples such as CAMB [9], CLASS [10], Colossus [11], CCL [12], and NumCosmo [13].

As previously noted, the large volume of data and the complexity of modeling cosmological probes necessitate optimized algorithms to enable feasible statistical analyses. Optimization methods often rely on techniques to approximate or estimate target functions and related operations, such as differentiation and integration. Interpolation techniques, including polynomial, spline, radial basis function interpolations [14, 15], and Gaussian processes [16, 17], are widely used for this purpose. In particular, the numerical analyses performed by these libraries often require evaluating computationally intensive functions. To reduce this workload, interpolation methods are employed: the expensive function is computed at a limited number of points, while the remaining values are estimated through interpolation. This approach plays a crucial role in the efficiency and development of these libraries.

A key consideration when using an interpolation method is determining the number and placement of knots. Minimizing the number of knots is crucial to reducing the computational cost of both evaluating the interpolation and the underlying high-cost function. At the same time, enough knots must be allocated to achieve the desired precision of the approximation. The placement of knots also affects the quality of the interpolation, as poorly chosen positions can lead to inefficiencies or inaccuracies in regions where the function changes rapidly [18]. Various techniques for optimizing knot allocation have been studied [19–21]. For example, [22] propose using a genetic algorithm to minimize a knot-dependent cost function, [23] apply an elitist clonal selection algorithm, and [24] utilize a Multi-Objective Genetic Algorithm. These approaches aim to balance computational efficiency with the precision of the interpolated function.

In most cases, users must manually configure the knot distribution, which can be both challenging and time-consuming. This process involves selecting the number and positions of knots, a task that becomes particularly difficult when the function to be interpolated is unknown or exhibits complex behavior. In cosmology and astrophysics, the optimal knot distribution often depends on the underlying model. For instance, the cosmological distance-redshift relation varies with cosmological parameters, and the number of knots needed for interpolation can change accordingly.

This dependence complicates the determination of an optimal knot distribution, especially during statistical analyses like Markov Chain Monte Carlo (MCMC), where model parameters are sampled from a probability distribution. In such cases, the knot configuration must ensure the desired precision across the full range of sampled parameter values. Moreover, in practical analyses in these fields, tens of functions often require interpolation, leading to a proliferation of configuration parameters that further increase the complexity and workload for the user.

In this work, we present a deterministic adaptive knot allocation method guided by two convergence criteria and a specified interpolation error threshold. This method ensures

that in statistical analyses, such as Markov Chain Monte Carlo, the approximated function achieves the desired precision consistently across the entire parameter space. The algorithm is implemented in the Numerical Cosmology library (NumCosmo [13]), an open-source library dedicated to cosmological and astrophysical computations, as well as statistical tools for data analysis.¹ Written in C and equipped with a Python interface, the library is designed to be accessible to a wide range of users. The algorithm undergoes rigorous testing and validation through extensive unit tests, ensuring its accuracy and reliability.

This paper is organized as follows. In section 2, we describe our deterministic method for automatic knot placement (AutoKnots), detailing the convergence criteria, parameters, and available options. In section 3, we evaluate the algorithm through a series of tests on diverse target functions, highlighting its performance across different scenarios. In section 4, we demonstrate the method’s application in a cosmological context by computing the surface mass density and mean surface mass density for two halo density profiles. Finally, section 5 presents our concluding remarks, while Appendix A defines cubic splines and outlines the steps for implementing the algorithm.

2 The adaptive method

The AutoKnots selection technique presented in this study is broadly applicable to various interpolation methods. To demonstrate its effectiveness, we focus on cubic spline interpolation with the not-a-knot condition [25]. For further details on cubic spline interpolation and the algorithm design, see Appendix A.

2.1 Definitions

Let $f(x)$ represent the function to be interpolated over the interval $[a, b]$. The set of strictly increasing knots and their corresponding function values denoted by \mathbb{K}^t :

$$\mathbb{K}^t = \{(x_0, f(x_0)), (x_1, f(x_1)), \dots, (x_n, f(x_n))\}, \quad (2.1)$$

where $x_0 = a$ and $x_n = b$, $n + 1$ is the number of knots, and t is the iteration number. Using these, the approximated function for a given interpolation technique is expressed as:

$$\hat{f}^t(x) \equiv \hat{f}(x|\mathbb{K}^t). \quad (2.2)$$

The interval $[a, b]$ is divided into n sub-intervals based on the knots, with their sizes defined as:

$$\mathbb{H}^t = \{h_0, h_1, \dots, h_{n-1}\}, \quad h_i \equiv x_{i+1} - x_i. \quad (2.3)$$

To test the accuracy of the interpolation $\hat{f}^t(x)$, we compare it to the true function $f(x)$ by evaluating both at a new set of points. To select these points, we use the midpoint rule, that is, for a given sub-interval $[x_i, x_{i+1}]$, we define the midpoint \bar{x}_i as:

$$\bar{x}_i = \frac{x_i + x_{i+1}}{2}. \quad (2.4)$$

The accuracy of the interpolation is then measured by the absolute error between the true function and its approximation:

$$\Delta^a f^t(x) \equiv \left| f(x) - \hat{f}_n^t(x) \right|. \quad (2.5)$$

¹<https://github.com/NumCosmo/NumCosmo>

For cubic spline interpolation with the not-a-knot condition, the error typically scales as $\mathcal{O}(h^4)$, where h is the size of the sub-interval. However, the exact error also depends on the specific function being interpolated and the sub-interval, with a proportionality constant that varies accordingly.

An additional test involves comparing the integral of the true function over the sub-intervals with the integral of the interpolated function. Although we do not have the exact integral, we can approximate it using Simpson’s 1/3 rule (see, for example, [26]):

$$\tilde{\mathcal{I}}_i = \frac{h_i}{6} [f(x_i) + 4f(\bar{x}_i) + f(x_{i+1})]. \quad (2.6)$$

This approximation also has an error of $\mathcal{O}(h^4)$, allowing us to compare the interpolation error with the integral error. The key advantage of this approach is that it provides a different proportionality constant, which helps identify regions where the interpolation is less accurate than the integral approximation or vice versa. We represent the integral of the interpolated function and its absolute difference from the Simpson’s 1/3 rule approximation as

$$\hat{\mathcal{I}}_i^t \equiv \int_{x_i}^{x_{i+1}} \hat{f}^t(x) dx, \quad \Delta^a \mathcal{I}_i^t \equiv \left| \tilde{\mathcal{I}}_i - \hat{\mathcal{I}}_i^t \right|. \quad (2.7)$$

Given a tolerance δ and a scale parameter ε , we define a point as having an interpolation error within the required precision if the following conditions are satisfied:

$$\Delta^a f^t(\bar{x}_i) < \delta [|f(\bar{x}_i)| + \varepsilon], \quad (2.8a)$$

$$\Delta^a \mathcal{I}_i^t < \delta \left[\left| \tilde{\mathcal{I}}_i \right| + \varepsilon h_i \right]. \quad (2.8b)$$

We track the status of each sub-interval using a set of integer variables

$$\mathbb{S}^t = \{s_0^t, s_1^t, \dots, s_{n-1}^t\}, \quad (2.9)$$

where s_i represents whether the sub-interval $[x_i, x_{i+1})$ is well approximated by the interpolation using the current set of knots. If $s_i^t = s_{\text{conv}}$, the sub-interval is considered well approximated; if $s_i^t < s_{\text{conv}}$, the sub-interval requires further subdivision.

2.2 Adaptive Algorithm

The AutoKnots algorithm is designed to automatically determine the optimal number and placement of knots based on the interpolation error criteria defined in eqs. (2.8). Under the not-a-knot condition, our cubic spline algorithm requires a minimum of six knots for interpolation [25]. In the initial step, we distribute these six knots uniformly across the interval $[a, b]$, forming the initial set \mathbb{K}^0 .

Since the behavior of the function $f(x)$ is unknown – specifically whether it exhibits regions of high variability or sharp changes—we begin with a uniform knot distribution. At this stage, it is uncertain whether $f(x)$ can be accurately approximated by a cubic spline with six equally spaced knots. To initiate the adaptive process, all s_i^0 values are set to zero.

Now, we begin the adaptive process. Given the sets \mathbb{K}^t and \mathbb{S}^t , we iterate over the sub-intervals. If $s_i < s_{\text{conv}}$, we apply the midpoint rule to generate a test point \bar{x}_i within the sub-interval $[x_i, x_{i+1})$. We then update the knot set to $\mathbb{K}^{t+1} = \mathbb{K}^t \cup \{(\bar{x}_i, f(\bar{x}_i))\}$ and evaluate the error criteria in eqs. (2.8) for both the function and its integral.

After updating to \mathbb{K}^{t+1} , the sub-interval $[x_i, x_{i+1})$ is subdivided into two new sub-intervals:

$$[x_j = x_i, x_{j+1} = \bar{x}_i), \quad [x_{j+1} = \bar{x}_i, x_{j+2} = x_{i+1}).$$

The set \mathbb{S}^{t+1} is updated as follows: if the conditions in eqs. (2.8) are satisfied for both the function and its integral, the new sub-intervals are assigned $s_i^t + 1$. Otherwise, the value of s_i^t is retained. This can be expressed as:

$$s_j^{t+1} = s_{j+1}^{t+1} = \begin{cases} s_i^t + 1, & \text{if conditions in eqs. (2.8) are satisfied,} \\ s_i^t, & \text{otherwise.} \end{cases}$$

This process is repeated until all sub-intervals are well approximated, meaning $s_i = s_{\text{conv}}$ for all i . The final set of knots \mathbb{K}^{t+1} is then used to compute the final approximation $\hat{f}^{t+1}(x)$. In the next sections we refer to the final approximation as $\hat{f}(x)$.

In summary, the algorithm improves the interpolation by adaptively sampling the function $f(x)$ in subregions where the criteria in eqs. (2.8) are not met within s_{conv} iterations. In these intervals, the midpoint rule is used to generate test points, though other strategies were also explored, such as using Chebyshev points [27] or identifying regions of high curvature. Among these, the midpoint rule proved to be the most efficient and effective approach. The adaptive process continues until all subregions satisfy the criteria, at which point the final approximation is computed. Furthermore, we observed that setting $s_{\text{conv}} > 1$ typically results in unnecessarily high accuracy, leading to more knots than required.

In the algorithm, the two precision parameters are initialized by the user (see the description of the code in section A.2). We tested various values for s_{conv} and found that the algorithm is robust when $s_{\text{conv}} = 1$. Again, using larger values typically results in more knots than necessary. Therefore, from this point onward, we will consistently use $s_{\text{conv}} = 1$.

2.3 Tolerance and Scale Parameters

The inclusion of the scale parameter ε in the convergence criteria serves a well-known purpose in numerical computations: it prevents issues that arise when the relative error becomes ill-defined. Specifically, if $\varepsilon = 0$, the convergence criteria rely solely on relative differences, that is,

$$\Delta^a f(\bar{x}_i) < \delta |f(\bar{x}_i)|, \quad \Delta^a \mathcal{I}_i < \delta \left| \tilde{\mathcal{I}}_i \right|. \quad (2.10)$$

In regions where $|f(\bar{x}_i)| \rightarrow 0$, the relative error is undefined, and the algorithm would continue refining the sub-intervals indefinitely, adding unnecessary knots without ever satisfying the conditions. This results in over-sampling the region and inefficient computations.

By introducing $\varepsilon > 0$, the convergence criteria gain an absolute threshold that stabilizes the process when $|f(\bar{x}_i)|$ is small. In these regions, the criteria are no longer driven to zero but instead bounded by the user-defined ε , avoiding numerical instability and ensuring practical convergence.

For regions where $|f(\bar{x}_i)| \gg \varepsilon$, the ε -dependent terms become negligible, and the criteria revert to being dominated by relative differences. This ensures that the algorithm maintains appropriate relative accuracy for larger function values, while remaining robust near zero.

In practice, ε allows users to specify the scale of function values that are relevant to their problem. This simple adjustment is especially useful for functions that span multiple orders of magnitude, ensuring balanced performance across all regions of the domain.

An important property of the cubic spline interpolation algorithm (under the not-a-knot condition) is its behavior under scalar multiplication of the function. If the original function is scaled by a constant factor, $f_A(x) = Af(x)$, the interpolated function also scales proportionally, $\hat{f}_A(x) = A\hat{f}(x)$. This is a direct result of the algorithm solving a linear system to determine the cubic polynomials within each interval. Consequently, the interpolation and its *relative* errors remain invariant under scalar transformations.

Condition (2.10) reflects this invariance: for $f_A(x)$, it becomes

$$\Delta^a f_A(x) = |A|\Delta^a f(x) < \delta|A||f(x)|.$$

While the absolute difference threshold is scaled by $|A|$, the relative error and the knot distribution remain unchanged. This property also ensures that the adaptive method does not distinguish between $f(x)$ and $-f(x)$, as only the magnitude of the function influences the placement of knots. Note that the same behavior is observed for the integral error criterion. When incorporating the scale parameter ε , condition (2.8a) transforms to

$$\Delta^a f_A(x) = |A|\Delta^a f(x) < \delta|A|(|f(x)| + \varepsilon/|A|).$$

To preserve the same knot distribution for $f_A(x)$ and $f(x)$, ε must scale by $|A|$, that is, $\varepsilon \rightarrow |A|\varepsilon$.

When $|f(\bar{x}_i)| \ll \varepsilon$, the convergence criteria reduce to:

$$\Delta^a f(\bar{x}_i) < \delta\varepsilon,$$

and

$$\Delta^a \mathcal{I}_i < \delta\varepsilon h_i.$$

In this regime, the error bounds become independent of the actual value of $f(\bar{x}_i)$. The absolute difference of the function is only required to be smaller than the product of the relative tolerance, δ , and the scale parameter, ε . Similarly, the integral error bound corresponds to approximating the integral as a rectangle with width h_i and height ε . This behavior ensures that in regions where the function magnitude is much smaller than ε , any interpolated value is effectively accepted as long as it satisfies these constant bounds.

This scenario often arises when interpolating functions like the Gaussian distribution, where tails extend far from the peak. In such regions, the function values are negligible, and relative error becomes irrelevant. The scale parameter ε effectively defines an absolute threshold, below which differences are ignored, prioritizing the efficiency of the interpolation process over precision.

When ε acts as an absolute tolerance, scaled by the relative tolerance δ , it sets the baseline for the acceptable error. In the extreme case where $\varepsilon \rightarrow \infty$, the convergence criteria are trivially satisfied at the initial iteration. This leads to a uniform distribution of knots (11 in total: six initial and five added in the first iteration) and results in an interpolation that does not adapt to the function's structure. Consequently, the resulting approximation becomes suboptimal, ignoring essential variations in the function.

2.4 Error Analysis

The error in cubic spline interpolation within a interval of width h_i is bounded by [28]:

$$\Delta^a f_i \sim \frac{1}{384} \left| f^{(4)} \right|_i h_i^4, \quad (2.11)$$

where $f^{(4)}$ represents the maximum fourth derivative of the function within the interval. This expression highlights how the interpolation error depends on the fourth derivative and the interval width h_i , with the error scaling as h_i^4 . This relationship ensures that reducing h_i significantly decreases the interpolation error, especially in regions where $f^{(4)}$ is large. Errors tend to be more pronounced near the endpoints due to the additional constraints imposed by cubic spline interpolation [29, 30].

To assess the convergence of the integral condition (2.8b), note that it compares two approximations of the function integral. Simpson's 1/3 rule has an associated error bound given by [26]:

$$\int_{x_i}^{x_{i+1}} f(x) dx - \tilde{\mathcal{I}}_i \sim -\frac{1}{2880} \left| f^{(4)} \right|_i h_i^5.$$

The cubic spline integral error bound within the interval h_i is given by [31]:

$$\int_{x_i}^{x_{i+1}} f(x) dx - \hat{\mathcal{I}}_i \sim -\frac{1}{180} \left| f^{(4)} \right|_i h_i^5.$$

This relation also underestimates the error of the cubic spline integral in intervals near the boundaries, similar to the function approximation. Combining both estimates, the theoretical absolute difference between these two estimators, *i.e.*, the error bound of condition (2.8b), is given by,

$$\Delta^a \mathcal{I}_i \sim \frac{1}{192} \left| f^{(4)} \right|_i h_i^5. \quad (2.12)$$

For the entire interval $[a, b]$, the maximum interpolation error takes a similar form [32]:

$$\Delta^a f(x)_{[a,b]} \sim \frac{5}{384} \left| f^{(4)} \right|_{[a,b]} \max_i \{h_i\}^4.$$

This expression provides an approximate upper bound for the global interpolation error. If a uniform knot distribution is assumed, it can be used to estimate the number of knots required to achieve a target error. For instance, for the function $f(x) = \cos(x)$ over $0 \leq x \leq \pi$, the maximum fourth derivative is $|f^{(4)}| = 1$. Targeting a maximum interpolation error of 10^{-8} , the optimal interval width can be approximated as:

$$h \sim \left[\frac{384 \Delta^a f(x)_{[0,\pi]}}{5 |f^{(4)}|_{[0,\pi]}} \right]^{1/4} \approx 0.03, \quad (2.13)$$

implying the use of approximately 100 knots.

While this calculation offers insights into the relationship between h , $f^{(4)}$, and the error, it presents two significant challenges. First, it requires prior knowledge of the fourth derivative, which may not be readily available for many functions. Second, assuming a uniform distribution of knots is often suboptimal, especially for functions with regions of rapid variation or sharp features.

To address these limitations, the adaptive method applies the error conditions (2.8a) and (2.8b) independently to each interval h_i , relying only on evaluations of the function and its integral. By iteratively adjusting the partitions h_i based on local error estimates, the adaptive method naturally produces a nonuniform distribution of knots, refining them in regions of high variability and spacing them farther apart in smoother regions. This ensures a more balanced and accurate approximation compared to a uniform distribution.

Moreover, the error bound for numerical integration combines the interpolation error and the error from Simpson’s rule, both of which scale as $f^{(4)} \times h_i^4$ but are evaluated at different points within the interval. This dual consideration ensures that the adaptive method efficiently captures the range of errors, minimizing discrepancies across the interval and enhancing the robustness of both interpolation and integration.

Concerning the convergence condition given in eq. (2.8b), Simpson’s 1/3 rule is chosen due to its balance between accuracy and computational efficiency. It is exact for polynomials of degree two and, as discussed, its error aligns well with that of cubic spline interpolation. This ensures a good level of accuracy for the integral estimates. Additionally, Simpson’s rule is straightforward to implement and computationally efficient, making it suitable for applications where multiple integrations are required. Therefore, the practical balance between simplicity and accuracy provided by Simpson’s 1/3 rule makes it a reliable choice.

Alternative numerical integration rules for condition (2.8b) would affect convergence behavior differently. Methods that are less aligned with the cubic spline integral approximation, such as the trapezoidal or Boole’s rules [26], would result in slower convergence, requiring more iterations than with the proposed condition, resulting in a less accurate approximation. Conversely, using a numerical integration method more closely aligned with the cubic spline, such as the modified Simpson’s rule [33, 34], could lead to faster convergence, requiring fewer iterations, but with a trade-off of reduced precision in the approximation and additional computational overhead.

2.5 The refine option

One of the main challenges in automatic knot allocation arises when the function contains regions with sharp features embedded in an otherwise relatively smooth background. In such cases, the sharp feature may fall entirely within one sub-interval, while the function appears nearly flat elsewhere. This issue became evident during tests, which revealed instances where the method failed to achieve the desired accuracy, particularly in regions of nearly zero curvature, such as inflection points. Here, the adaptive method can converge prematurely, effectively overlooking the sharp feature and producing a suboptimal knot distribution.

A similar issue is encountered in adaptive quadrature methods, where algorithms may fail to adequately sample regions containing singularities or abrupt changes in the function’s behavior. These failures occur because the algorithm’s convergence criteria can be satisfied without sufficiently refining the partition in these problematic areas, leading to inaccurate results. Addressing this challenge requires additional safeguards or modifications to the adaptive method to ensure that regions with sharp features receive the necessary refinement.

To address this issue, we introduce the **refine** option, a heuristic approach designed to improve accuracy in regions where premature convergence might have occurred. The process begins by running the adaptive method until all sub-intervals satisfy the convergence criteria in eqs. (2.8), resulting in $s_i = s_{\text{conv}}$ for all sub-intervals.

If the **refine** option is enabled, we then compute the mean $\text{mean}(H^{t+1})$ and standard deviation $\text{std}(H^{t+1})$ of the sub-interval widths, h_i , across all sub-intervals. Next, we evaluate the following condition:

$$h_i > \text{mean}(H) + \text{refine_ns} \times \text{std}(H), \quad (2.14)$$

where **refine_ns** is a user-defined parameter controlling the sensitivity of the refinement. If this condition is met for a sub-interval $[x_i, x_{i+1})$, we reset $s_i = 0$ for that sub-interval and restart the adaptive method.

This refinement procedure is repeated for the number of iterations specified by the user. By iteratively refining intervals with unusually large widths, the `refine` option ensures that regions with sharp features are better resolved, reducing the likelihood of premature convergence and improving the overall accuracy of the method.

The use of standard deviation is intentional, as its sensitivity to outliers helps identify intervals with significant deviations from the average width. The user-defined parameter, `refine_ns`, determines the threshold in units of $\text{std}(H)$ for targeting regions that require additional knots. As `refine_ns` increases, the `refine` option becomes less sensitive, affecting only the most extreme partitions. Beyond a certain value, the threshold effectively disables refinement. Selecting an appropriate `refine_ns` requires balancing sensitivity to outliers with the need to avoid excessive refinement, with moderate initial values often providing satisfactory results.

The user can specify the number of iterations for grid refinement using the parameter `refine`, an unsigned integer. If `refine` is set to zero, no grid refinement is performed, and only the adaptive method is applied (see Section 2), bypassing condition (2.14). For `refine` ≥ 1 , condition (2.14) is evaluated iteratively up to `refine` times. This process progressively generates a more uniformly distributed grid with increased knot density as `refine` increases or `refine_ns` decreases, until condition (2.14) is satisfied or the maximum number of knots, specified by the input parameter `max_nodes`, is reached.

It is worth noting that the `refine` option does not directly pinpoint regions of premature convergence, which may result in the addition of unnecessary knots and increased precision. While increasing s_{conv} could also address this issue, our tests revealed that it often leads to over-sampling and reduced efficiency. By contrast, the `refine` option offers a more targeted strategy for improving accuracy in regions with sharp features, enhancing the overall performance of the adaptive method.

3 Testing AutoKnots

In this section, we present a series of numerical tests to evaluate the adaptive methodology described in section 2. The tests are divided into two parts. First, we analyze three distinct functions: a smooth function to demonstrate the basic application of the adaptive method, a function with sharp features to explore the impact of the `refine` option, and a function with varying scales to highlight the influence of the scale parameter. Second, we assess the method’s overall behavior and stability by applying it to three different sets of functions, each generated randomly ten million times with variations in specific parameters.

For each test, the approximated functions, $\hat{f}(x)$, are compared to the true functions, $f(x)$, using a uniformly spaced linear grid with ten thousand (10,000) nodes. This grid resolution ensures that all relevant properties of the functions are adequately captured, providing a reliable benchmark for evaluating the performance of the adaptive method.

The input parameter values remain consistent: the relative tolerance, δ , is set to 10^{-8} , and the scale parameter, ε , is set to 0 unless otherwise specified. The relative difference between the function, $f(x)$, and the approximated function, $\hat{f}(x)$, is computed using the following expression, which incorporates the scale parameter, ε when present:

$$\Delta^r f(x) = \frac{\Delta^a f(x)}{|f(x)| + \varepsilon}, \quad (3.1)$$

where $\Delta^a f(x)$ is defined in eq. (2.5). The relative difference between the integral of the function, I , and the integral of the approximated function, $\hat{I}(N)$, across their interval is also

estimated:

$$\Delta^r Q = \left| \frac{I - \hat{I}}{I} \right|, \quad (3.2)$$

where I is the exact integral and \hat{I} is the integral of the approximated function. This parameter is intended to evaluate the overall behavior of the approximation produced by the adaptive method. It's important to note that this definition does not incorporate the scale parameter ε to evaluate its impact.

The AutoKnots algorithm produces several metrics to assess its performance, each reflecting a key aspect of the method's accuracy and efficiency. These metrics are:

- **Number of Knots:** Represents the total number of knots in the final approximation, which indicates the computational complexity of the solution.
- **Fails:** The percentage of nodes in the linear grid that exceed the specified relative tolerance. This metric quantifies the extent to which the approximation deviates from the desired accuracy at specific points.
- **Normalized Maximum Relative Difference, $\Delta^r f(x)_{\max}/\delta$:** The maximum relative difference between the approximated and true functions across the grid, normalized by the relative tolerance δ . A value larger than one indicates that the method failed to achieve the desired accuracy in some regions, whereas a value significantly smaller than one suggests overestimation of the number of knots.
- **Maximum Relative Difference in Integral, $\Delta^r Q$:** Evaluates the accuracy of the integral approximation. This metric is crucial for assessing the overall performance, as the method is not solely an interpolator but also a quadrature estimator.

These metrics collectively provide a comprehensive picture of the method's performance, balancing accuracy and efficiency. By analyzing these outputs, users can identify whether the algorithm has failed, overestimated, or achieved an optimal knot distribution.

3.1 The Adaptive Method Applied to a Smooth Function

The first function analyzed is the natural logarithm, $f(x) = \ln(x)$, evaluated over the interval $2 \leq x \leq 10$. The adaptive method generates a distribution of knots that is denser in regions of higher curvature and sparser in regions of lower curvature. As x increases, the curvature diminishes, and the knot density decreases accordingly, as illustrated in figure 1.

Interestingly, slight peaks in knot density are observed at the boundaries of the interval. This behavior is attributed to the reduced precision of cubic spline interpolation near boundary knots, a known limitation associated with additional conditions at the edges [29, 30]. Despite this, the approximated function successfully maintains the desired tolerance throughout the entire interval. The maximum relative difference, $\Delta^r \ln(x)_{\max}/\delta = 0.66$, is well within the specified tolerance. Additionally, the function meets all precision requirements, as detailed in the second row of table 1.

For comparison, using eq. (2.13) with an absolute difference matching the requirement of condition (2.8a), $\Delta^a \ln(x)/\delta \approx 0.7$ for $x = 2$, results in approximately 230 evenly distributed knots. The value at $x = 2$ was chosen because the fourth derivative of $f(x) = \ln(x)$ is maximized at this point, making it the most stringent region for the error condition. In contrast, the adaptive method achieves the same precision with significantly fewer knots.

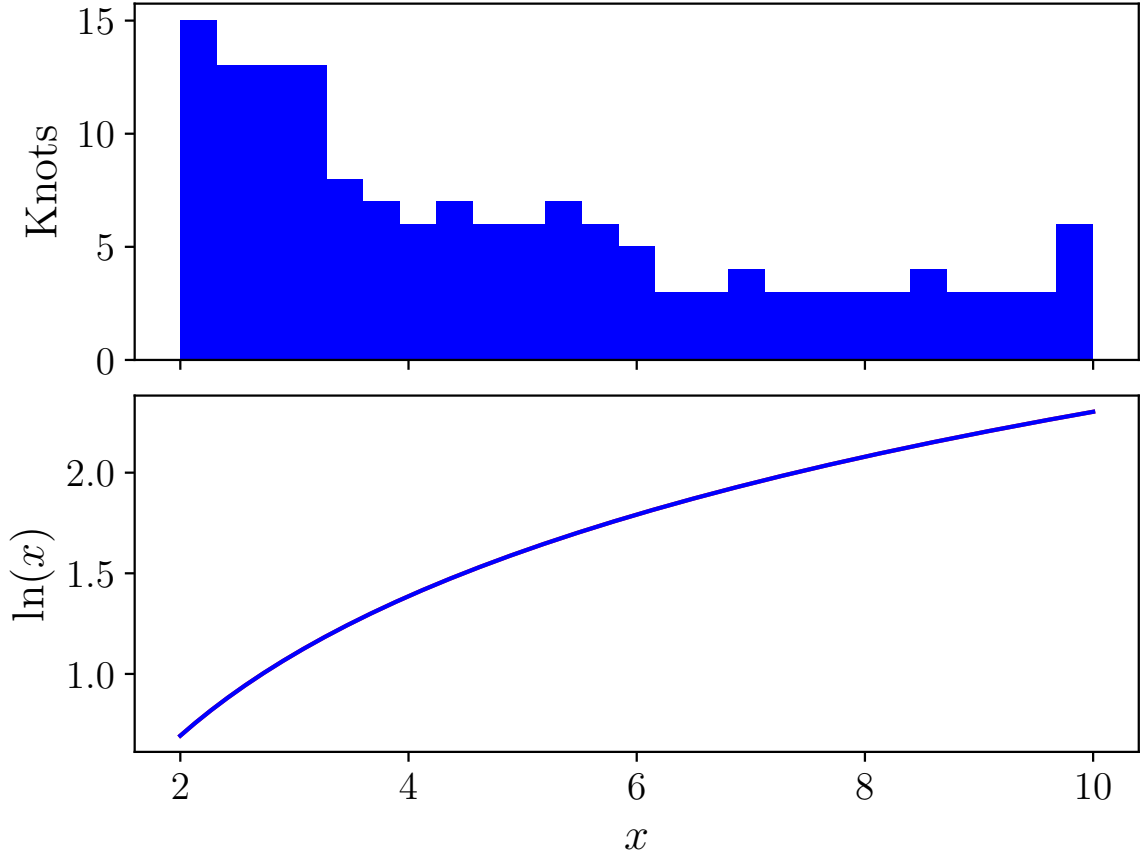


Figure 1. The lower plot depicts the function $f(x) = \ln(x)$, while the upper plot illustrates the knot distribution generated by the AutoKnots algorithm.

$f(x)$	Knots	Fails	Δ_{\max}^r/δ	Δ_{\max}^a/δ	$\Delta^r Q/\delta$
$\ln(x)$	153	0.00%	0.66	0.53	0.013
$I_d(x)$	927	1.24%	5.90	0.71	0.038
	945	0.00%	0.43	0.06	0.002
$N(x)$	2249	0.00%	0.17	0.08	0.002
	457	0.42%	0.12	1.27	0.023
	313	0.00%	0.13	1.33	0.120
	169	0.00%	0.68	68.1	11.10

Table 1. Numerical results for the AutoKnots method applied to the three test functions: $\ln(x)$ (section 3.1), $I_d(x)$ (section 3.2), and $N(x)$ (section 3.3). The second column reports the total number of knots generated. The third column indicates the percentage of grid nodes that fail to meet the convergence criteria. The fourth and fifth columns present the maximum relative and absolute differences, respectively, across all grid nodes. The sixth column shows the integral relative difference, as defined in eq. (3.2). For $I_d(x)$, the first row corresponds to results obtained using the adaptive method alone, while the second row includes results with `refine` set to 1 and `refine_ns` set to 2.5. For $N(x)$, results are shown for the adaptive method with scale parameters $\varepsilon = 0, 1, 10, \text{ and } 100$, listed sequentially from top to bottom.

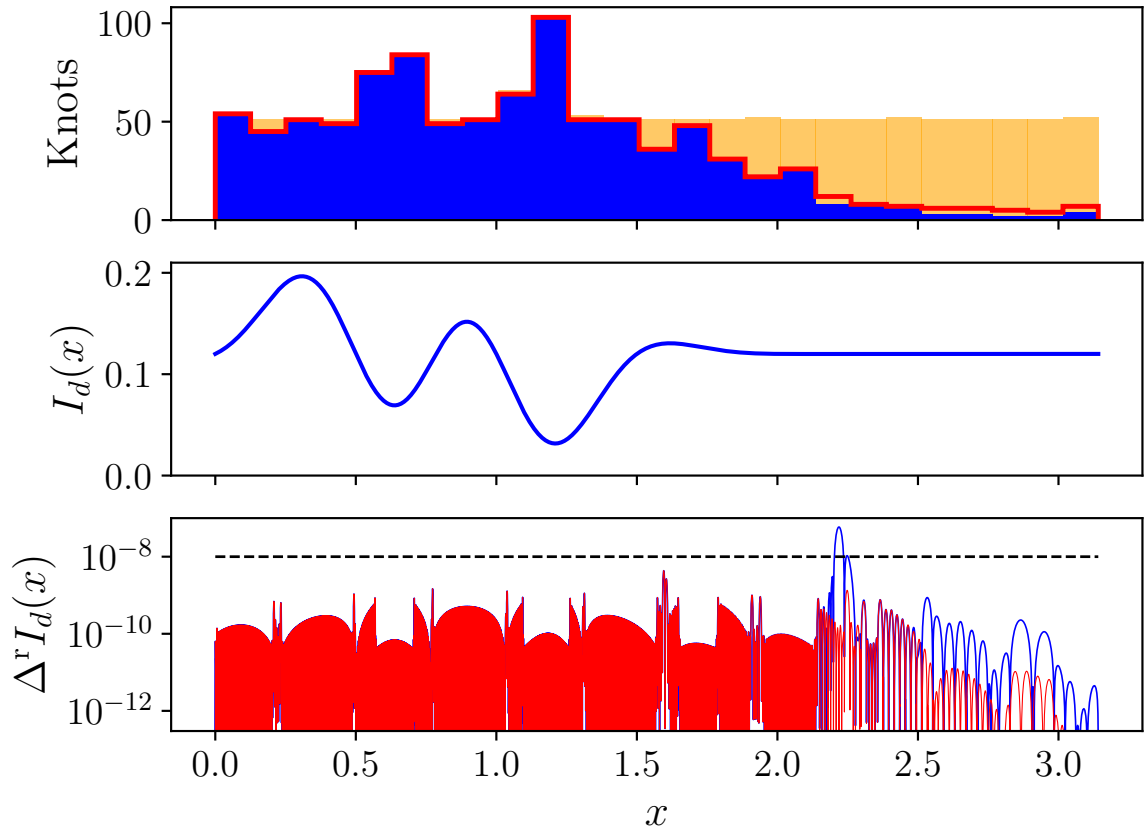


Figure 2. The function $I_d(x)$, defined in eq. (3.3), is depicted in the middle plot. The bottom plot shows the relative difference, $\Delta^r I_d(x)$, at each grid node, with the black dashed line representing the convergence threshold. The top plot illustrates the knot distribution: results from the adaptive method are represented by the blue line and blue-filled histogram, those with `refine` = 1 and `refine_ns` = 2.5 are depicted by the red line and red step histogram, and results with `refine` approaching infinity and `refine_ns` = 1 are shown by the orange-filled histogram.

3.2 Testing the refine option

To evaluate the effectiveness of the `refine` option, we analyze a function with contrasting behaviors: rapid oscillations in one region and a nearly constant plateau in another. This provides a challenging test case for adaptive methods, particularly in identifying and refining problematic regions.

The function under consideration is given by

$$I_d(x) = 0.12 + 0.25 \exp \left[-4(x - \pi/4)^2 \right] \cos(2x) \sin(2\pi x), \quad (3.3)$$

and is evaluated in the interval $0 \leq x \leq \pi$. This function, previously used by [24] to test a Multi-Objective-Genetic Algorithm (MOGA) for knot placement in cubic spline interpolation, combines high-frequency oscillations near the start of the domain with a smooth plateau in the latter half, as shown in the middle plot of figure 2.

Figure 2 illustrates results obtained with three configurations of the input parameters:

1. Baseline Adaptive Method: The adaptive method alone is applied, represented by the blue line/filled histogram. This results in a higher density of knots in the oscillatory region and fewer in the plateau.
2. Limited Refinement: The AutoKnots algorithm is enhanced with the `refine` option set to 1 and `refine_ns` set to 2.5, shown as a red line/step histogram. Values of `refine_ns` up to 5 yield the same outcome, while higher values effectively disable the refinement process.
3. Aggressive Refinement: The `refine` parameter is set to a very high value, with `refine_ns` set to 1, depicted by the orange-filled histogram. When pushed to the extreme, the refinement process minimizes the variance of the interval widths, effectively making all intervals as small as the smallest one before the refinement starts.

These configurations demonstrate how the `refine` option influences knot distribution, improving accuracy in complicated regions while balancing efficiency.

The relative difference, $\Delta^f I_d(x)$, is shown in the bottom plot of figure 2, while numerical results for the first two evaluations are presented in the third and fourth rows of table 1, respectively. The adaptive method fails to meet the specified tolerance within a narrow segment near the transition to the plateau, with 1.24% of the grid nodes exceeding the desired tolerance. The fourth and sixth columns of table 1 show the maximum relative difference on the linear grid, $\Delta^f I_d(x)_{\max}/\delta = 5.9$, which is within an order of magnitude of the convergence criterion, and the integral relative difference, $\Delta^f Q/\delta = 0.0378$, which falls below the convergence criterion. These results demonstrate that the adaptive method provides a precise approximation of the true function.

To achieve not only accuracy but also compliance with the convergence criteria across the entire interval, the `refine` option becomes useful. This option is specifically designed to address situations where small deviations from the required tolerance must be minimized. By probing intervals with widths larger than the average, the `refine` option can identify and correct these regions. The top plot of figure 2 shows the distribution of knots, illustrating that setting `refine` to 1 with `refine_ns` set to 2.5 increases the knot density within the plateau region and extends the refinement to all nodes that fail to meet the tolerance. However, this also results in the introduction of unnecessary knots for $x > 2.5$. As shown in the first column of table 1, this configuration leads to a 2% increase in the total number of knots, which in turn reduces the maximum relative difference to 4.3×10^{-9} , well within the desired tolerance of 10^{-8} .

When the number of refinements `refine` is large and `refine_ns` is set to 1, the knot distribution becomes nearly uniform across the second half of the function, targeting all intervals that meet condition (2.14). This analysis highlights the effect of excessive refinement values on knot distribution. However, such an approach is not recommended, as it results in oversampling, making all intervals as small as the smallest interval before refinement starts. Consequently, numerical results for this configuration are omitted from table 1, and its relative difference is not included in figure 2.

3.3 Scale Parameter

The third test case illustrates the role of the scale parameter, ε , in controlling interpolation accuracy. The scale parameter serves two primary purposes: (i) it defines an absolute tolerance for functions passing through zero, ensuring the adaptive process terminates even when

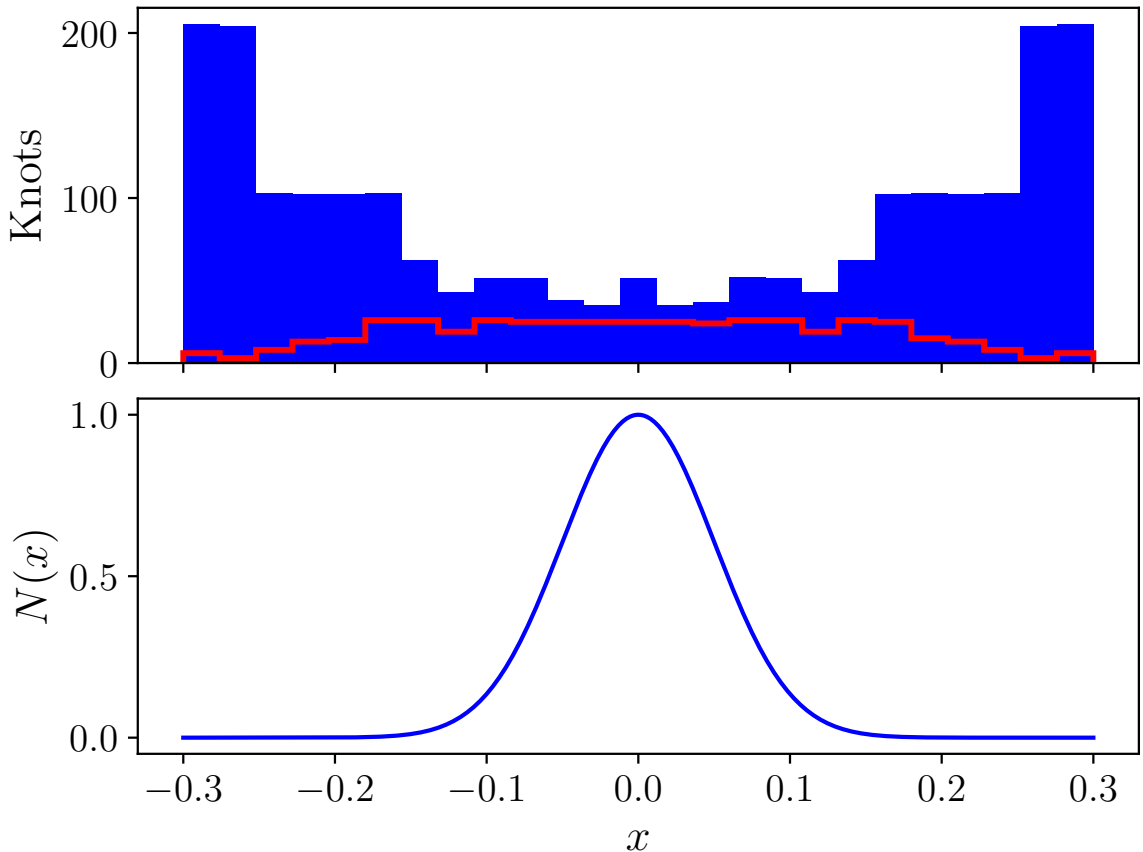


Figure 3. The function $N(x)$ given by eq. (3.4) is depicted in the bottom plot. The top plot displays the distribution of knots, where the blue-filled histogram represents the adaptive method with $\varepsilon = 0$, and the red step histogram represents $\varepsilon = 1$.

$f(x_0) = 0$ for $x_0 \in [a, b]$, and (ii) it allows users to deprioritize regions where the function magnitude is negligible when compared to the scale parameter. This is particularly useful for functions with significant variations in magnitude, as it reduces the number of knots in regions where the function is small, focusing computational resources on areas with more significant values.

To demonstrate these effects, we employ the Gaussian function:

$$N(x) = \exp\left[-\frac{1}{2}\left(\frac{x}{0.05}\right)^2\right], \quad (3.4)$$

evaluated over the interval $-0.3 \leq x \leq 0.3$.

The bottom plot in figure 3 shows $N(x)$, while the top plot displays the knot distributions for $\varepsilon = 0$ (blue-filled histogram) and $\varepsilon = 1$ (red step histogram). When $\varepsilon = 0$, the number of knots increases rapidly as $|N(x)|$ approaches zero, consistent with the behavior described in section 2. Numerical results for $\varepsilon = 0, 1, 10$, and 100 are summarized in rows five through eight of table 1. As ε increases, the number of knots decreases significantly, reflecting reduced sensitivity to regions where $|N(x)| \ll \varepsilon$.

For the scale parameter $\varepsilon = 0$, the maximum relative and absolute differences are $\Delta^r N(x)_{\max}/\delta = 0.17$ and $\Delta^a N(x)_{\max}/\delta = 0.08$, respectively, indicating that the required accuracy is achieved. In this case, the tails of the function are accurately approximated, as the scale parameter is not introduced. The integral relative difference is $\Delta^r Q/\delta = 0.002$, indicating an over-sampled approximation. This is expected, as the method is designed to ensure accuracy in the function tail, even when $N(x)$ is negligible.

For $\varepsilon = 1$, the maximum relative difference remains consistent with the absolute tolerance, $\Delta^r N(x)_{\max}/\delta = 0.12$. In regions where $N(x) \ll 1$, particularly near the tails of the function, the error threshold effectively becomes $\Delta^a N(x)_{\max} < \delta(\varepsilon + |N(x)|) \approx 10^{-8}$. For instance, if $N(x_0) = 10^{-9}$ and $\hat{N}(x_0) = 2 \times 10^{-9}$, the relative error with $\varepsilon = 0$ would be $\Delta^r N(x_0) = 1$, prompting the AutoKnots method to add more knots to meet the convergence criteria. In contrast, with $\varepsilon = 1$, the same error would result in $\Delta^r N(x_0) \approx 10^{-9}$, which falls well within the tolerance, and the adaptive method would not increase the number of knots. This demonstrates how ε prevents over-sampling in regions where $N(x)$ is negligible when compared to the scale parameter. Naturally, the absolute difference is not necessarily smaller than one, in this case, $\Delta^a N(x)_{\max}/\delta = 1.27$. This is consistent with the absolute tolerance threshold.

To illustrate the effects of choosing ε larger than the maximum value of $N(x)$, we analyze cases where $\varepsilon = 10$ and $\varepsilon = 100$. When $\varepsilon > \max N(x)$, the relative tolerance δ is effectively reduced, leading to a global decrease in interpolation precision. For $\varepsilon = 10$, this reduction is modest, as the value is only one order of magnitude larger than $\max N(x)$, resulting in a reasonably accurate approximation. However, for $\varepsilon = 100$, the effects are more pronounced, with $\Delta^a N(x)_{\max}/\delta = 68.1$ and $\Delta^r Q/\delta = 11.10$, indicating an approximation that fails to meet the desired tolerance anywhere within the domain, see the last row of table 1. This highlights the importance of carefully selecting ε to balance precision and efficiency.

The choice of ε should align with the scale of the smallest function values of interest to achieve the best results. For $N(x)$, while $|N(x)|_{\max} = 1$, the optimal outcome was obtained with $\varepsilon \approx 1$, highlighting that both the function's maximum value and the desired balance between accuracy and efficiency play a role in determining the appropriate scale parameter.

To assess the impact of a function crossing the abscissa, we studied the function $N_o(x) = 10N(x) - 5$, evaluated within the same interval. The amplitude and offset values were chosen to minimize the impact of the scale parameter beyond the abscissa crossing. Figure 4 illustrates the function and the distribution of knots for $\varepsilon = 0$ and $\varepsilon = 1$. The impact of the scale parameter is noticeable only where the function crosses the abscissa. The number of knots is similar, decreasing by 9% from 733 to 669, and both approximated functions share the same maximum absolute difference. This demonstrates that the AutoKnots algorithm is not highly sensitive to this type of behavior.

For comparison, we also analyzed the $\ln(x)$ and $I_d(x)$ functions (see section 3.1 and section 3.2) using $\varepsilon = 1$. For $\ln(x)$, the number of knots decreased slightly, from 153 to 135, with negligible changes in all other parameters. The function $I_d(x)$ exhibited a more pronounced effect, with the number of knots reduced significantly from 927 to 539, while the maximum absolute difference remained nearly unchanged. This variation arises because $I_d(x)_{\max} \approx 0.2$, making the absolute tolerance dominant in the optimization process, whereas $\ln(x = 2) \approx 0.7$, causing $\varepsilon = 1$ to affect only the beginning of its interval. In practice, determining the optimal ε value is often challenging, as it depends on the function's behavior and may involve parameters unknown *a priori*. Hence, it is generally advisable to set $\varepsilon = 0$ or choose the smallest value that still captures the function's features accurately.

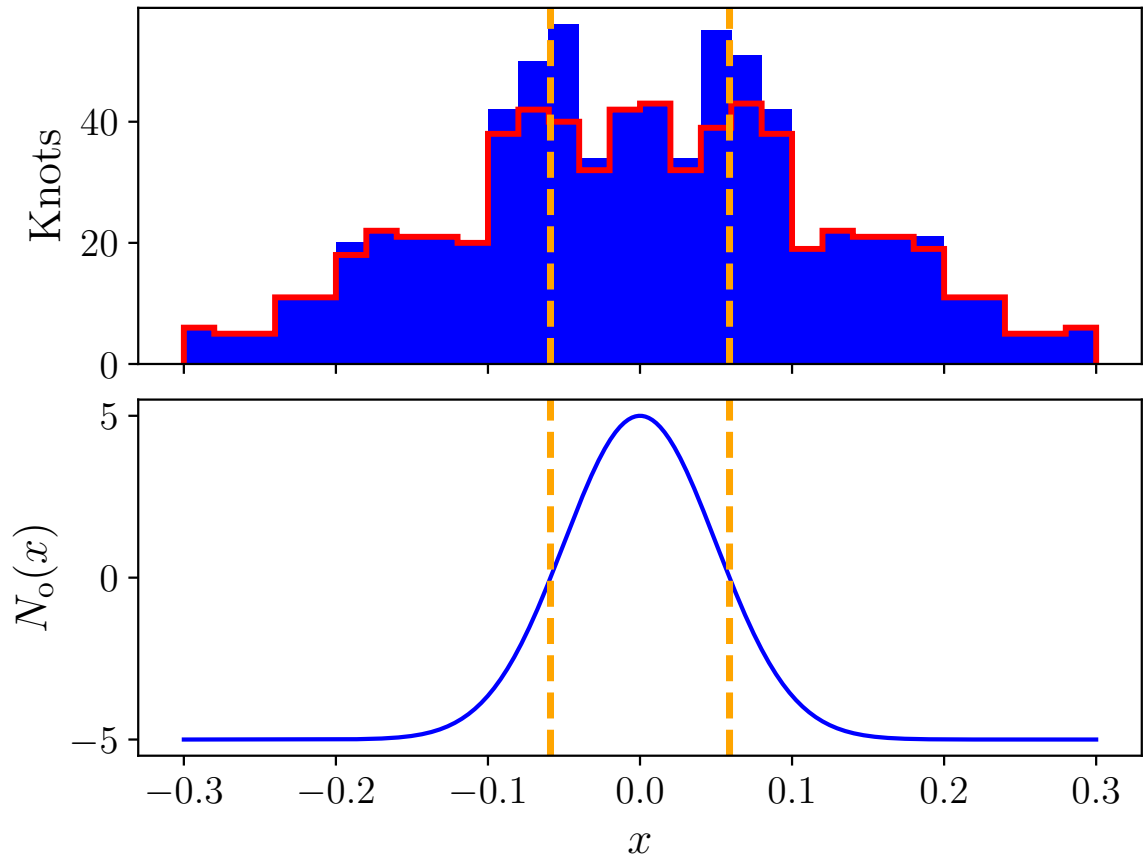


Figure 4. The function $N_o(x) = 10N(x) - 5$ is depicted in the bottom plot. The top plot displays the distribution of knots: the blue-filled histogram represents the adaptive method with $\varepsilon = 0$, and the red step histogram represents $\varepsilon = 1$. The vertical orange dashed lines in both plots indicate where the function crosses the abscissa.

These results underscore the difficulty of selecting an optimal scale parameter for a given function. There is no universal method to determine the ideal ε value, and its choice typically requires trial and error, as illustrated with the Gaussian function. Choosing $\varepsilon = 0$ is a conservative approach that guarantees a fit within the desired tolerance but can result in over-sampling under certain conditions. It is worth noting that $\varepsilon = 0$ corresponds to setting the absolute tolerance to zero in other numerical techniques, such as quadrature methods, thereby demanding a similar balance between precision and efficiency.

3.4 Statistical Performance Evaluation

In this section, we evaluate the statistical performance of the AutoKnots method by applying it to a broad set of parametrized functions with randomly sampled parameters. The goal is to test the algorithm’s robustness and versatility across a diverse range of functional forms, simulating scenarios where function parameters are inferred from data, such as in optimization techniques like maximum likelihood estimation or Markov Chain Monte Carlo. To this end, we generate ten million (10^7) random samples from three distinct sets of functions and compare

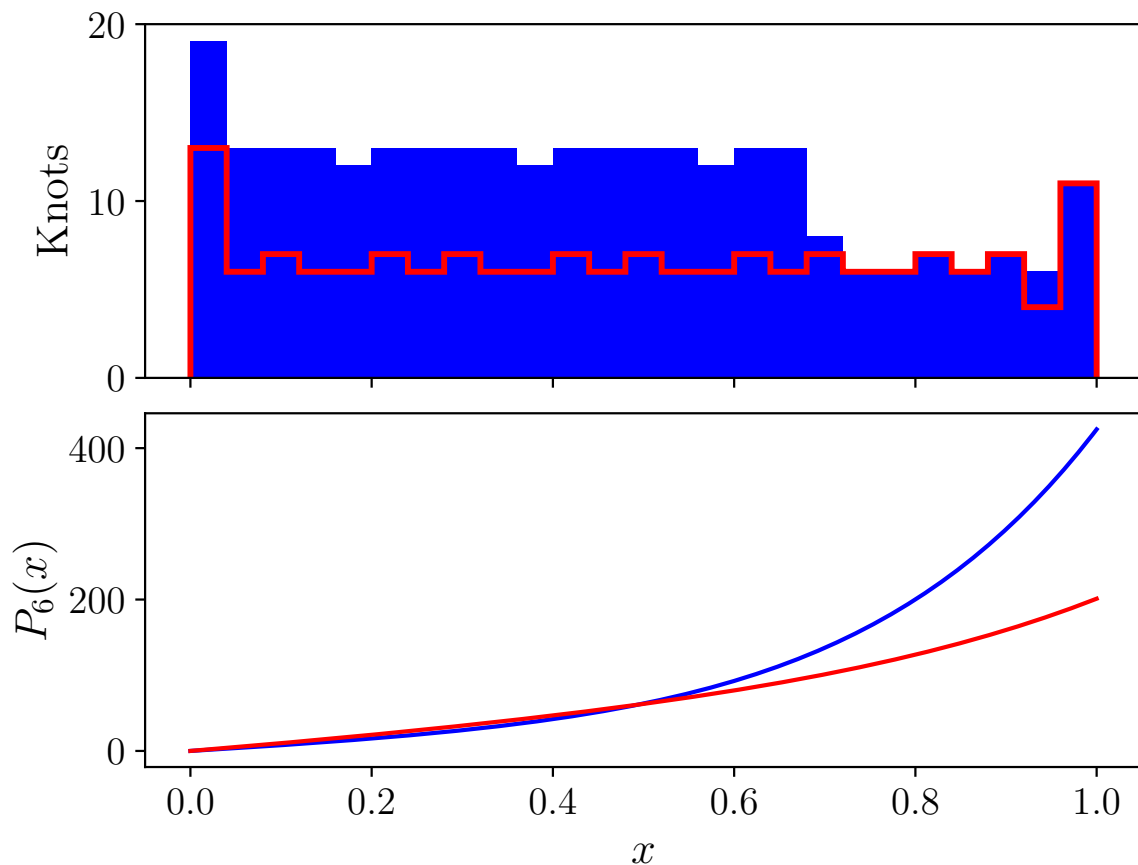


Figure 5. The lower plot illustrates two realizations of the function $P_6(x)$, defined by eq. (3.5), while the upper plot displays their respective knot distributions generated by the adaptive method.

$f(x)$	Refine	Knots	Fails	$\frac{\Delta^f f(x)_{\max}}{\delta}$	MAX
$P_6(x)$	(0, 0)	260 ± 51.9	0.3%	0.7 ± 9	500
$P_6(x)$	(1, 5)	260 ± 52.2	0%	0.2 ± 0.1	0.9
$P_6(x)$	(1, 1)	291 ± 64.4	0%	0.2 ± 0.08	0.4
$C_s(x)$	(0, 0)	1070 ± 218	40%	$9 \pm 4 \times 10^3$	7×10^6
$C_s(x)$	(1, 5)	1080 ± 220	4%	0.4 ± 0.4	50
$C_s(x)$	(1, 1)	1180 ± 251	0.002%	0.07 ± 0.04	50
$E_s(x)$	(0, 0)	625 ± 186	20%	3 ± 300	3×10^3
$E_s(x)$	(1, 5)	627 ± 186	4%	0.4 ± 1	30
$E_s(x)$	(1, 1)	689 ± 188	0.002%	0.1 ± 0.09	20

Table 2. Numerical results for the adaptive method applied to the functions $P_6(x)$ (eq. (3.5)), $C_s(x)$ (eq. (3.6)), and $E_s(x)$ (eq. (3.7)). The second column specifies the refinement applied. The third column presents the mean and standard deviation of the number of knots generated across all realizations. The fourth column reports the percentage of realizations that failed to meet the convergence criteria (Fails). The fifth column provides the mean and standard deviation of the maximum relative error for all realizations. Finally, the last column shows the absolute maximum relative error across all realizations.

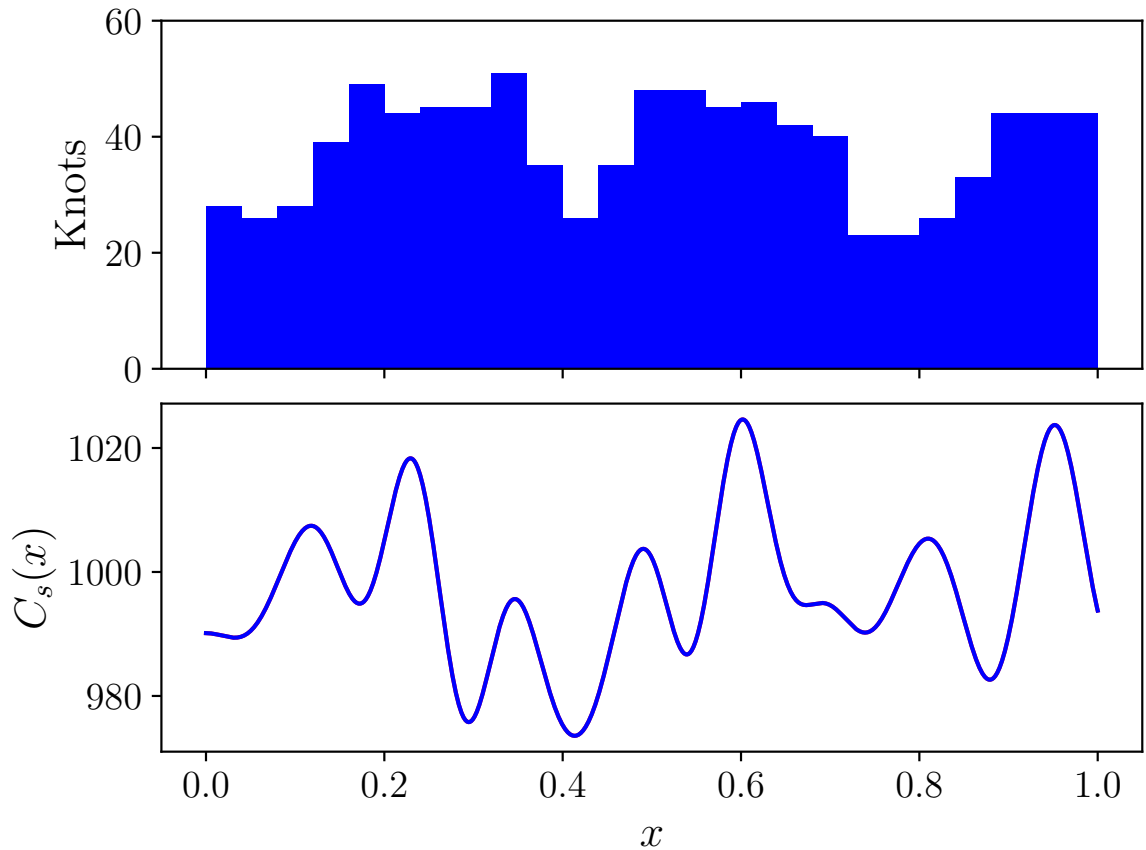


Figure 6. The lower plot illustrates a single realization of the function $C_s(x)$ defined by eq. (3.6), while the upper plot shows the knot distribution generated by the adaptive method.

the fitted results to the true functions using a uniform linear grid of ten thousand nodes for each realization. All analyses are performed over the interval $0 \leq x \leq 1$.

The evaluation is purely numerical, relying solely on the data obtained from the realizations without invoking any theoretical probability distribution for the parameters. It is assumed that the dataset of ten million realizations is sufficiently large to approximate the true distribution, enabling a reliable assessment of the method’s performance.

To evaluate the method’s performance across a wide range of functions, we focus on the following metrics:

- **Knots:** For each realization, we apply AutoKnots to the function and generate a distribution of knots. We then compute the mean and standard deviation of the number of knots across all 10^7 realizations for each function.
- **Fails:** For each realization, we compute the approximation and evaluate it on the grid, comparing the approximation to the original function. If the approximation at any grid point fails to recover the original function value within the desired tolerance, that realization is marked as failed. The reported percentage of failures (Fails) is the total number of failed realizations divided by 10^7 .

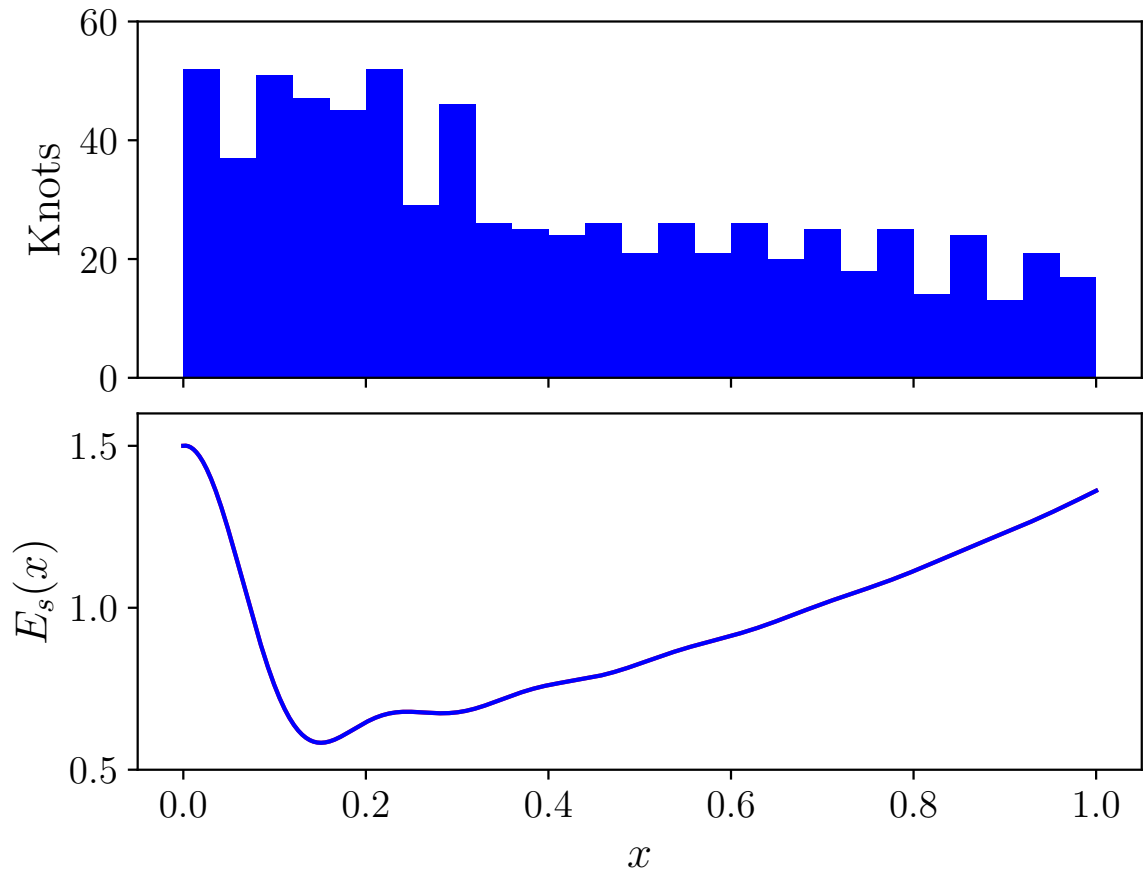


Figure 7. The lower plot illustrates a single realization of the function $E_s(x)$ defined by eq. (3.7), while the upper plot shows the knot distribution generated by the adaptive method.

- **Maximum Relative Difference:** For each grid point in a realization, we compute the relative difference as $\Delta^r f(x)_{\max}/\delta$. For each realization, we select the maximum relative difference across all grid points. Using these 10^7 maximum values, we compute the mean and standard deviation, as well as the maximum value across all realizations (MAX).

The adaptive method is tested on three sets of functions, each with distinct characteristics. For each set, we evaluate the method under three configurations: no refinement (0,0), one refinement with `refine_ns` = 5 (1,5), and one refinement with `refine_ns` = 1 (1,1).

The initial function is a sixth-order polynomial. This function set was specifically designed to assess the performance of the adaptive method on smooth functions. Its expression is as follows:

$$P_6(x) = \sum_{i=1}^6 A_i x^i. \quad (3.5)$$

In each realization, the parameters A_i are randomly drawn from a uniform distribution within $1 \leq A_i \leq 100$. It's noteworthy that all instances of $P_6(x)$ have a value of zero at $x = 0$ and

are increasing positive functions. Figure 5 illustrates two instances of $P_6(x)$, showcased in the lower plot, along with the corresponding distributions of knots depicted in the upper plot.

The second set of functions aims to assess the performance of the AutoKnots algorithm under conditions of high variability, defined as:

$$C_s(x) = \sum_{i=1}^{29} B_i \cos(2\pi\nu_i x) + 10^3. \quad (3.6)$$

The amplitudes B_i and frequencies ν_i are randomly sampled from a normal distribution with a mean of zero and a standard deviation of 5. The constant factor has an equivalent effect to adding the scale parameter with the same value, $\varepsilon = 1000$, influencing the absolute difference threshold as $\Delta^a C_s(x)_{\max} \approx 1000 \delta = 10^{-5}$. Figure 6 illustrates an instance of such realization, showcasing $C_s(x)$ in the lower plot and presenting the corresponding distribution of knots in the upper plot.

The third and final set of functions is given by:

$$E_s(x) = 0.5 e^{\alpha x} + \left[\frac{\sin(\beta x)}{\beta x} \right]^2, \quad (3.7)$$

The parameters α and β are randomly sampled from uniform distributions within the intervals $0.1 \leq \alpha \leq 2$ and $5 \leq \beta \leq 30$. Figure 7 displays an example of a realization with $\alpha = 1$ and $\beta = 20$. This function serves as an intermediary between the smoothness of $P_6(x)$ and the high variability of $C_s(x)$.

The numerical results of this analysis, summarized in table 2, highlight the relationship between function characteristics and the number of knots generated. As expected, the smooth function $P_6(x)$ requires fewer knots compared to the highly variable $C_s(x)$. The function $E_s(x)$, with intermediate smoothness and variability, falls between these two extremes.

3.4.1 Smooth Function $P_6(x)$

For $P_6(x)$, just 0.3% of the realizations fail to meet the tolerance when no refinement is applied. However, within these few cases, the maximum relative difference reaches 500, or about three orders of magnitude above the tolerance ($500 \times 10^{-8} = 5 \times 10^{-6}$). When one refinement with `refine_ns = 5` is applied, the failure rate drops to zero, and the maximum relative difference reduces to 0.2 ± 0.1 , with an absolute maximum of 0.9. This demonstrates excellent performance, achieving results very close to the desired tolerance without generating unnecessary knots. Increasing the refinement to `refine_ns = 1` results in a 12% increase in the number of knots. While the failure rate remains at zero, the maximum relative difference improves slightly to 0.2 ± 0.08 , with a reduced absolute maximum of 0.4. This configuration provides the best results, with nearly all realizations meeting the desired tolerance.

In figure 8, the plot illustrates the distribution of the maximum relative error for $P_6(x)$, highlighting a minor mode near $\Delta^r P_6(x) \approx 10^{-6}$, which corresponds to realizations that fail to meet the required tolerance. These realizations are better approximated when refinement is applied, demonstrating how the refinement process effectively identifies and corrects problematic regions. One last interesting aspect is that, for all applications of the algorithm, the approximations do not exceed the required tolerance by much more than one order of magnitude. This shows that the method does not use excessive knots, achieving efficient approximation without unnecessary complexity.

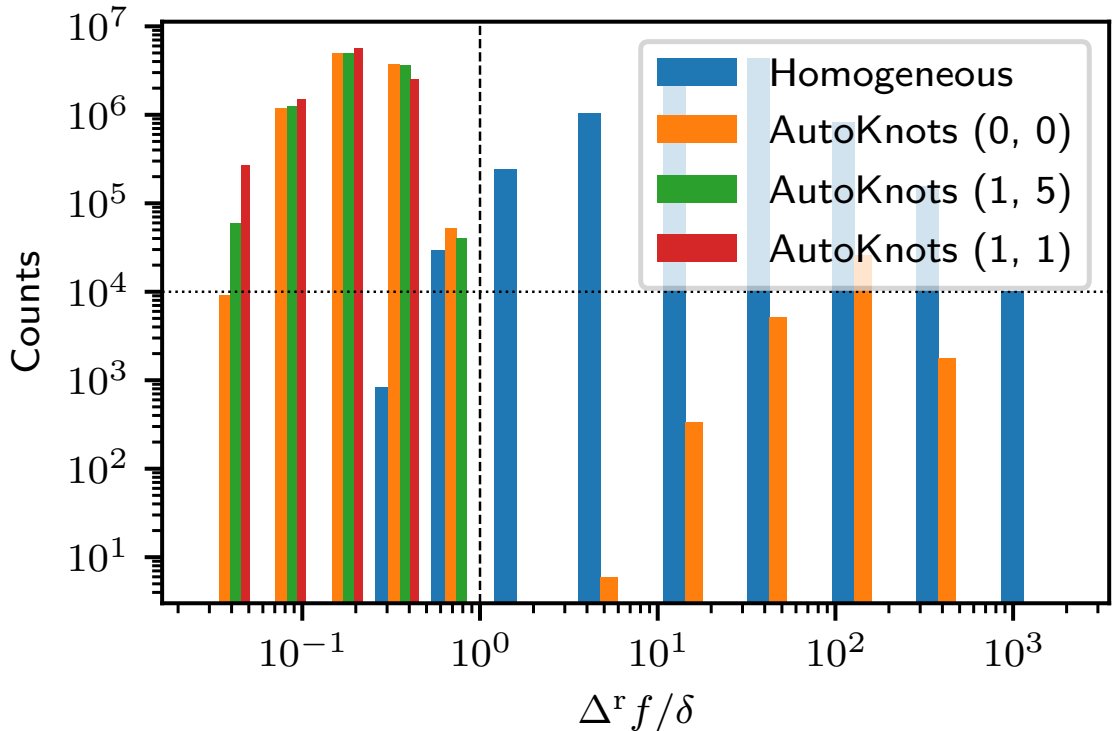


Figure 8. Histograms showing the distribution of the maximum relative error for $P_6(x)$. Bins to the right of 1 (vertical dashed line) correspond to failed realizations, while bins below the dotted line represent less than 0.1% of the total realizations. AutoKnots without refinement exhibits a second mode to the right of 1, indicating feature loss in some realizations. The refinement process shifts more realizations to the left, improving accuracy. A homogeneous knot distribution (with the same number of knots) performs significantly worse, with most bins to the right of 1. See figure 9 and figure 10 for similar analyses of $C_s(x)$ and $E_s(x)$.

3.4.2 Highly Variable Function $C_s(x)$

Now, let us discuss the results for $C_s(x)$. When no refinement is applied, the adaptive method generates several knots, with a mean of 1070 and a standard deviation of 218. The failure rate is 40%, with a maximum relative difference of $9 \pm 4 \times 10^3$ and an absolute maximum of 7×10^6 . These results indicate that the AutoKnots method with no refinement struggles to approximate the function accurately, with a significant proportion of realizations exceeding the desired tolerance.

When one refinement with `refine_ns = 5` is applied, the number of knots remains similar, with a mean of 1080 and a standard deviation of 220. The failure rate decreases to 4%, with a maximum relative difference of 0.4 ± 0.4 and an absolute maximum of 50. This configuration demonstrates a substantial improvement, with the majority of realizations now meeting the desired tolerance.

Increasing the refinement further to `refine_ns = 1` results in a 10% increase in the number of knots, with a mean of 1180 and a standard deviation of 251. The failure rate drops dramatically to 0.002%, with a maximum relative difference of 0.07 ± 0.04 and an absolute

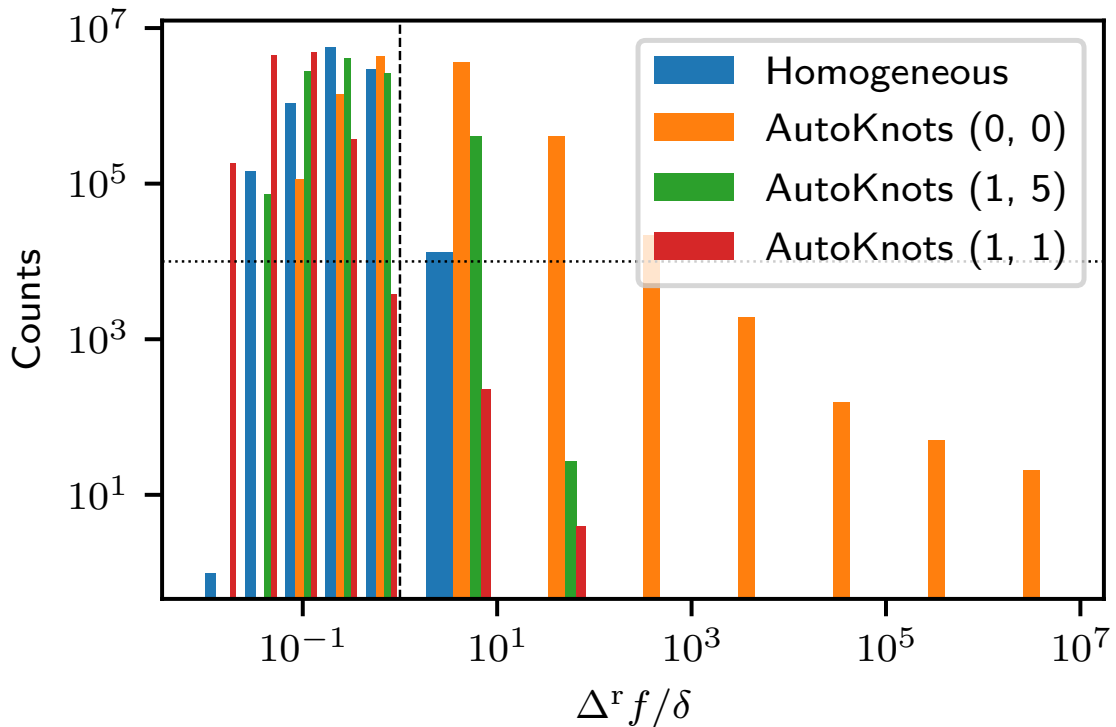


Figure 9. Histograms for the maximum relative error of $C_s(x)$, with the same conventions as figure 8. Without refinement, AutoKnots fail more often, showing a second mode to the right of 1. Refinement significantly improves performance, shifting realizations left. The homogeneous knot distribution performs better than AutoKnots without refinement but worse than AutoKnots with refinement, as seen by its higher failure rate and larger first bin to the right of 1.

maximum of 50. This configuration yields the best performance, with nearly all realizations meeting the desired tolerance.

One notable result for $C_s(x)$ is the surprisingly good performance of the homogeneous knot distribution, as shown in figure 9. It results in fewer failed realizations than the adaptive method without refinement and shows a better maximum relative difference. This is likely due to the periodic nature of the function, where the homogeneous distribution can capture the oscillations more efficiently than the adaptive method without refinement. However, since the homogeneous distribution uses the same number of knots as the adaptive method (derived from AutoKnots), it is not a fair comparison. In practice, one would need to know the optimal number of knots in advance.

When compared to AutoKnots with refinement, the homogeneous distribution performs worse. For example, the first bin to the right of 1 in the homogeneous distribution is significantly larger than in AutoKnots with (1, 1). This difference is reflected in the failure rates: 0.002% for AutoKnots with (1, 1) versus 0.1% for the homogeneous distribution.

3.4.3 Intermediate Function $E_s(x)$

For $E_s(x)$, the adaptive method without refinement uses an average of 625 knots (standard deviation: 186) and has a failure rate of 20%. The maximum relative error is 3 ± 300 , with

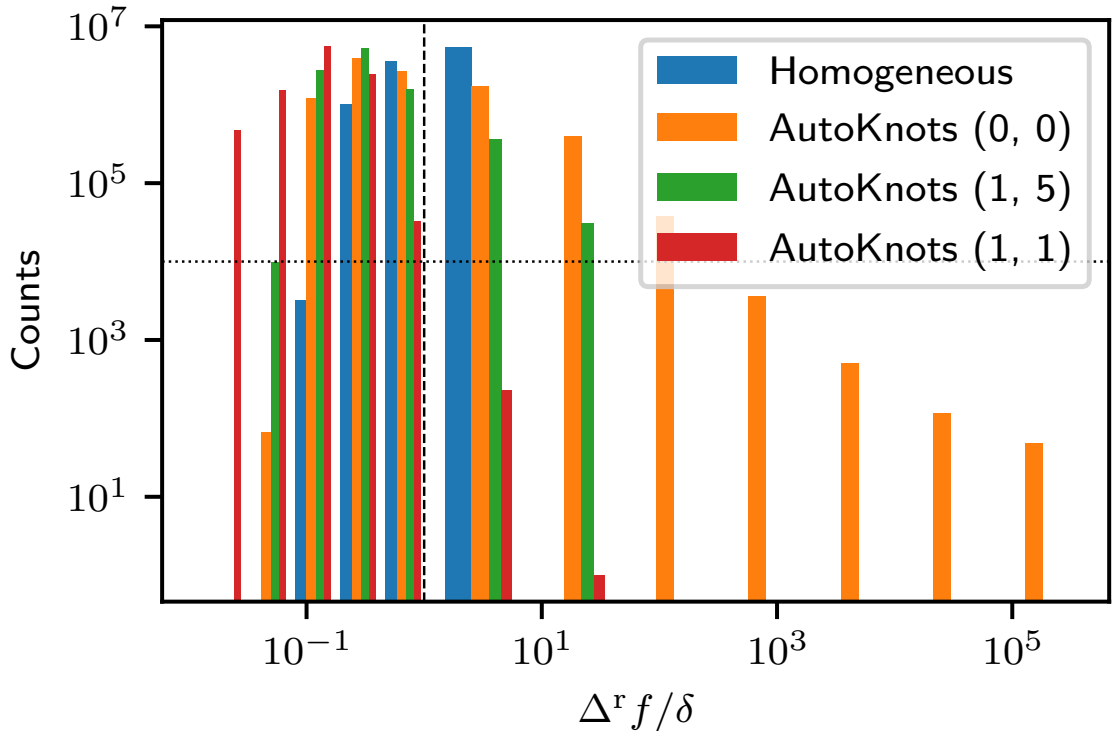


Figure 10. Histograms for the maximum relative error of $E_s(x)$, with conventions matching figures 8 and 9. Without refinement, AutoKnots exhibits a significant number of failed realizations and a second mode to the right of 1. Refinement reduces the failure rate and improves accuracy. The homogeneous knot distribution outperforms AutoKnots without refinement but performs worse than AutoKnots with refinement, showing higher failure rates and larger error bins.

an absolute maximum of 3×10^3 . Adding one refinement step (`refine_ns = 5`) maintains a similar knot count (mean: 627, standard deviation: 186) but reduces the failure rate to 4%. The maximum relative error drops significantly to 0.4 ± 1 , with an absolute maximum of 30. This shows that refinement substantially enhances performance, ensuring most realizations meet the tolerance.

Further increasing the refinement (`refine_ns = 1`) raises the average knot count by 10% (mean: 689, standard deviation: 188) and lowers the failure rate to just 0.002%. The maximum relative error becomes 0.1 ± 0.09 , with an absolute maximum of 20, yielding the best results with nearly all realizations meeting the tolerance.

Comparing the homogeneous knot distribution with AutoKnots, the homogeneous approach has a higher failure rate without refinement due to the function’s intermediate smoothness and variability, which the adaptive method captures more effectively. However, the homogeneous method achieves smaller maximum relative errors in some cases, suggesting better approximation for specific realizations. Even so, AutoKnots with refinement outperforms the homogeneous approach across all metrics, as shown in figure 10.

3.4.4 Refinement Analysis

Considering the results for $P_6(x)$, $C_s(x)$, and $E_s(x)$, the refinement process significantly improves the adaptive method’s performance. The number of knots remains relatively stable, with a slight increase when refinement is applied. For smooth functions like $P_6(x)$, the number of knots is increased by 12% when refinement is applied unnecessarily. However, for functions with higher variability, such as $C_s(x)$ and $E_s(x)$, the increase is necessary to ensure the desired tolerance.

The refinement process also reduces the failure rate, with the most significant improvement observed for $C_s(x)$, where the failure rate drops from 40% to 0.002% when refinement is applied. The maximum relative difference is also significantly reduced, with the absolute maximum falling from 7×10^6 to 50 for $C_s(x)$. This demonstrates the effectiveness of the refinement process in improving the adaptive method’s performance.

Naturally, if the function to be approximated is smooth, the refinement process may not be necessary, as seen in the case of $P_6(x)$. However, for functions with higher variability, such as $C_s(x)$ and $E_s(x)$, the refinement process is essential to ensure the desired tolerance is met. In general, the more conservative approach is to apply the refinement process, as it ensures the adaptive method performs well across a wide range of functions while only marginally increasing the number of knots. The default configuration used in NumCosmo is to apply one refinement with `refine_ns = 1`, as this provides the best results across all functions tested.

4 Applications in Cosmology

The AutoKnots algorithm has been integrated into various components of NumCosmo to streamline the configuration of cosmological models and calculations. By automating the choice of knot placement based on convergence criteria and interpolation error thresholds, AutoKnots reduces the need for manual tuning of configuration parameters, such as the number of knots. This capability is especially valuable in complex cosmological codes, where the range of required parameters can be extensive.

In this section, we discuss the range of applications of AutoKnots within NumCosmo, highlighting its versatility and effectiveness. We describe specific objects and functions that use the algorithm and provide detailed results of two applications. These examples illustrate how AutoKnots simplifies the setup of cosmological analyses while maintaining high precision and computational efficiency.

- **Map on a spherical shell:** The `NcmSphereMap` object² provides a set of functions dedicated to pixelating the spherical surface (sky), given a resolution, performing coordinate system transformations, and computing the a_{lm} coefficients of a spherical harmonics decomposition. It also calculates the two-point angular functions in real and Fourier spaces: $C(\theta)$ and C_l , respectively.³
- **Spherical Bessel (SB) function:** NumCosmo provides three methods to compute the SB function: a multi-precision version, an approximation up to the third order of the SB’s power series, and one using spline interpolation. The spline is built by calculating the knots from the multi-precision SB function.⁴

²`NcmSphereMap` is a re-implementation of the HEALPix code[35].

³In particular, the method `ncm_sphere_map_calc_Ctheta` is used to compute $C(\theta)$.

⁴The method for this is `ncm_sf_sbessel_spline`.

- **Filtered power spectrum:** This method computes a power spectrum $P(k, z)$ filtered by a window function, where k is the wave-number and z is the redshift. The calculation is optimized by constructing a bi-dimensional spline in k and z . The spline in k is derived using the Fast Fourier Transform of $P(k, z)$ with logarithmically spaced points (FFTLog) in the range $(\ln k_i, \ln k_f)$. The method `ncm_powspec_filter_prepare` is applied to compute the respective spline in z and its integral.
- **Correlation function in 3D:** The `NcmPowspecCorr3d` object computes the 3D two-point spatial correlation function from the filtered power spectrum. The method used is `ncm_powspec_corr3d_prepare`.
- **Halo mass function:** The `NcHaloMassFunction` object provides various functions, such as computing the number density of halos as a function of halo mass M and redshift z , i.e., $d^2N/dz d \ln M$, the halo distribution in z , dN/dz , and the total number of halos N given mass intervals and z . The 2D adaptive approach is used to build the 2D spline in z and $\ln M$ of the halo mass function.⁵
- **Perturbation:** The `NcHIPert` object solves the ordinary differential equations (ODE) for perturbations in spatially homogeneous and isotropic cosmologies. A common problem is determining the modes for which the ODEs should be solved to compute the power spectrum. This method offers a natural way to select the best knots for the required precision, a process typically done *a priori* in codes like CAMB. Our approach applies to the WKB approximation. The method used is `_nc_hipert_wkb_prepare_approx`.
- **Recombination:** The `NcRecomb` object describes the universe’s recombination period, specifically the fraction of light elements in various states and the number of free electrons. The adaptive method is used to compute the Seager implementation [36].⁶
- **Halo density profile:** The `NcHaloDensityProfile` object implements the matter halo density profile $\rho(r)$, the enclosed mass in a spherical volume given $\rho(r)$, the surface mass density $\Sigma(R)$, and the average surface mass density within a cylinder of radius R , $\bar{\Sigma}(< R)$. The last two functions use the adaptive method.⁷ These methods return the dimensionless surface mass density $\hat{\Sigma}(R)$ and the enclosed mass in an infinite cylinder, $\hat{\bar{\Sigma}}(< R)$, of radius R .

It is worth noting that the Firecrown⁸ and CLMM⁹ packages utilize certain NumCosmo tools that incorporate the AutoKnots algorithm. Firecrown and CLMM are official tools of the Dark Energy Science Collaboration (DESC) of the LSST. Reference [37] presents a comparison of the accuracy of various functions related to the matter halo density profile across CCL, Cluster Toolkit¹⁰, Colossus, and NumCosmo.

⁵The method is `_nc_halo_mass_function_generate_2Dspline_knots`.

⁶The method is `_nc_recomb_seager_prepare`.

⁷The methods are:

- `_nc_halo_density_profile_prepare_dl_2d_density`,
- `_nc_halo_density_profile_prepare_dl_cyl_mass`.

⁸<https://github.com/LSSTDESC/firecrown>

⁹<https://github.com/LSSTDESC/CLMM>

¹⁰<https://cluster-toolkit.readthedocs.io/en/latest/>

In the following, we evaluate the performance of the method by computing the dimensionless quantities $\hat{\Sigma}(R)$ and $\hat{\Sigma}(< R)$ for two different halo density profiles: the Navarro-Frenk-White (NFW) profile [38] and the Hernquist profile [39]. These profiles were selected because they both provide analytical expressions for $\hat{\Sigma}(R)$ and $\hat{\Sigma}(< R)$, allowing us to compare the results obtained using the adaptive method with the analytical solutions.

For each value of R , we compute the dimensionless surface mass density $\hat{\Sigma}(R)$ and the average surface mass density within a cylinder of radius R , $\hat{\Sigma}(< R)$, for both the NFW and Hernquist profiles. These calculations involve integrating the matter density profiles along the line of sight for $\hat{\Sigma}(R)$ and within the cylinder for $\hat{\Sigma}(< R)$. Since each new value of R requires fresh integrations, we utilize the AutoKnots algorithm to dynamically generate R values and their corresponding interpolated functions. This approach minimizes the number of knots and consequently the computational cost, while ensuring the desired precision.

We calculate $\hat{\Sigma}(R)$ and $\hat{\Sigma}(< R)$ with the relative tolerance δ ranging from 10^{-10} to 10^{-1} . For these functions, we apply the default refinement option. Additionally, as they are positive-definite, we set the scale parameter $\epsilon = 0$. In figure 11, we present the number of knots required and how it increases with the relative tolerance for the four cases considered. It is worth noting that the number of knots increases more rapidly when $\delta > 10^{-6}$.

In figures 12 and 13, we present the relative difference between the analytical and spline-interpolated results for $\hat{\Sigma}(R)$ and $\hat{\Sigma}(< R)$, respectively, for both NFW (upper panel) and Hernquist profiles (lower panel). In all cases, the interpolated functions achieve the required precision, typically exceeding one order of magnitude over the entire domain of R .

In practice, many cosmological functions do not have analytical solutions, even for other halo matter density profiles. Consequently, these computations rely on numerical methods such as integration and ordinary differential equation solvers, often combined with interpolation techniques. While many codes offer algorithms with hard-coded interpolation features, such as pre-defined knots, these are typically tested in specific scenarios. It is impractical to rely on these fixed algorithms to ensure the necessary numerical precision for statistical analyses, such as Markov Chain Monte Carlo (MCMC) sampling. The approach presented here addresses this limitation. For example, at each step of an MCMC run, the functions will meet the required numerical precision by dynamically generating the list of knots and constructing the corresponding interpolated functions.

5 Conclusions and Final Remarks

This work presents the AutoKnots algorithm, a novel adaptive method for automatic knot allocation in spline interpolation, designed to satisfy user-defined precision requirements. In contrast to traditional methods that require manually configured knot distributions with numerous parameters, the proposed approach automatically determines the optimal number and placement of knots based on interpolation error criteria.

In section 3, a series of numerical tests were conducted on the AutoKnots algorithm, demonstrating its consistent ability to accurately approximate the functions under analysis. While instances of premature convergence were observed in more complex functions, such as $C_s(x)$ and $E_s(x)$, where the adaptive method alone could not achieve the desired tolerance, the refinement process effectively mitigated these issues, significantly enhancing performance. The number of knots generated by the adaptive method remained relatively stable across different functions, with a slight increase when refinement was applied.

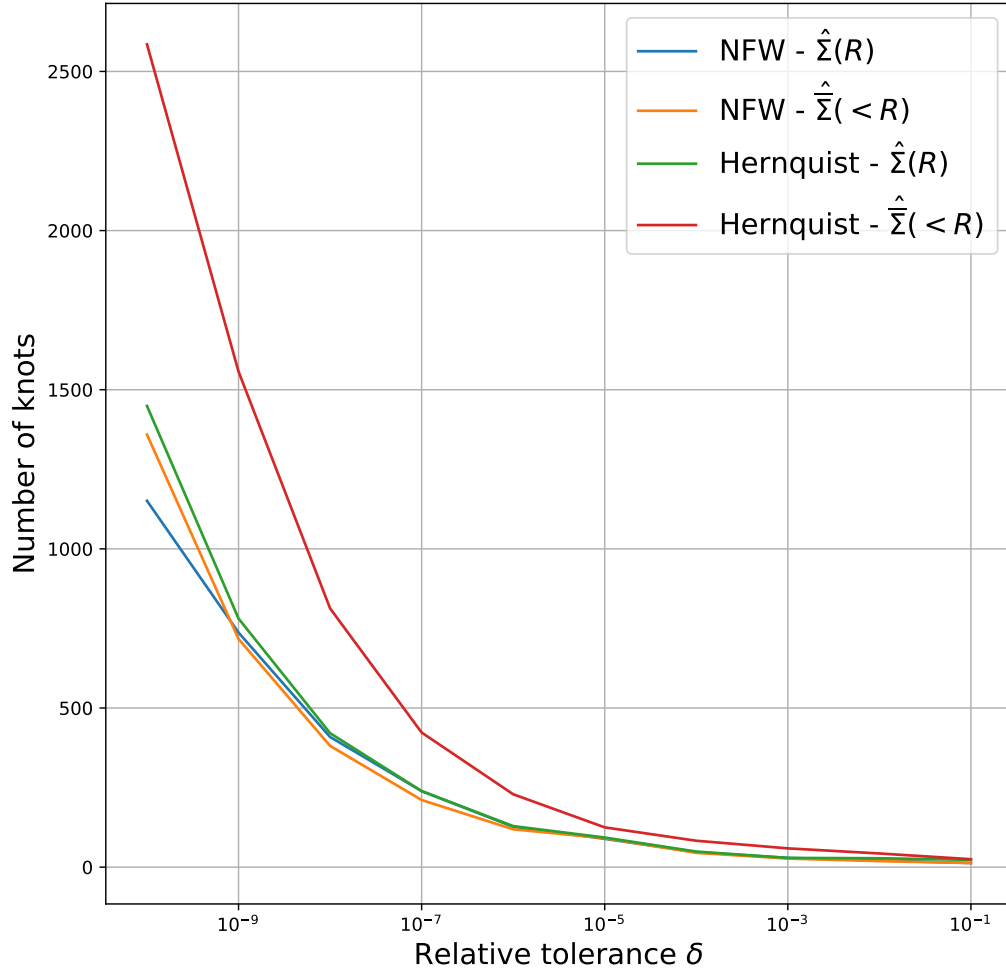


Figure 11. Number of knots as a function of the relative tolerance δ computed in the interval $\delta \in [10^{-10}, 10^{-1}]$ for the four cases: $\hat{\Sigma}(R)$ and $\hat{\Sigma}(< R)$ using NFW (blue and orange curves) and Hernquist (green and red curves) profiles. The plot illustrates how the number of knots increases with decreasing tolerance for both profiles.

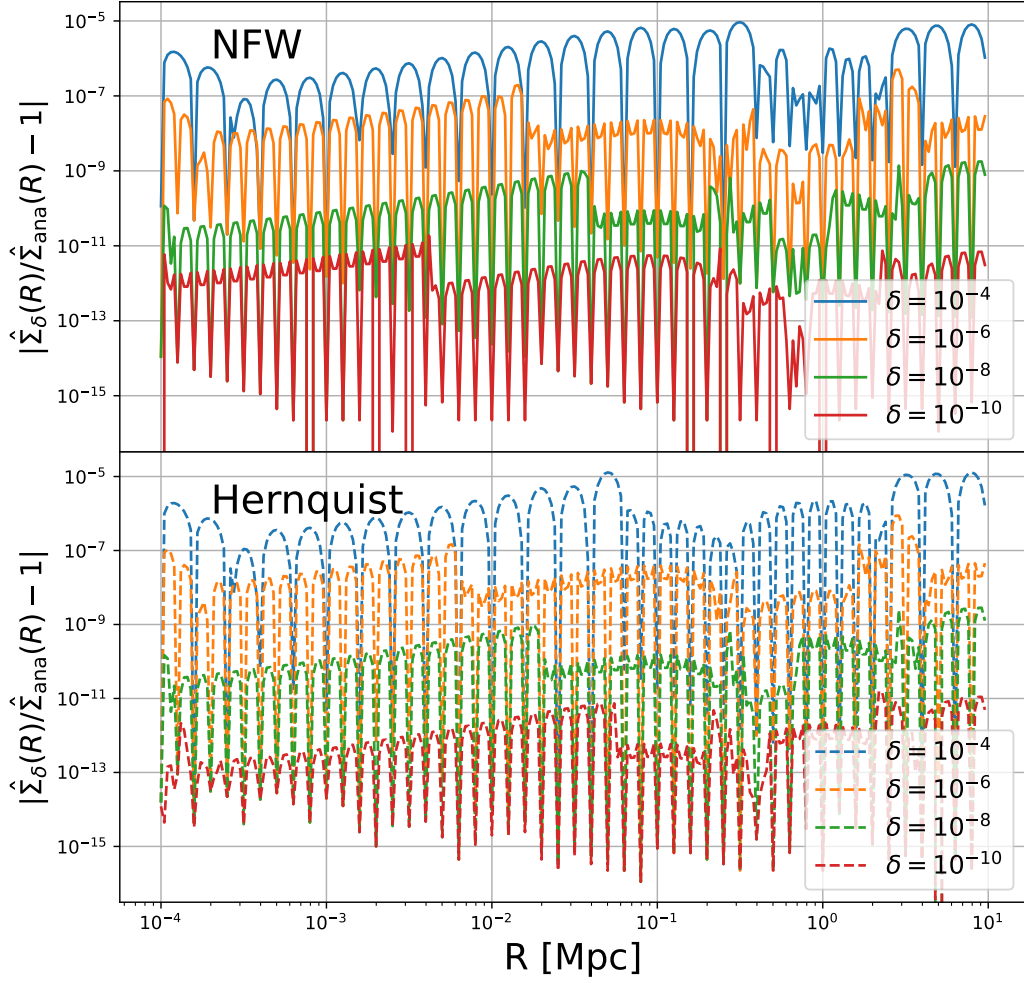


Figure 12. The relative difference between the dimensionless surface mass density $\hat{\Sigma}(R)$ computed using spline interpolation and analytically for the NFW matter density profile (upper panel) and the Hernquist profile (lower panel). In both cases, the splines were built requiring a relative tolerance δ equal to 10^{-4} , 10^{-6} , 10^{-8} and 10^{-10} corresponding to the blue, orange, green and red curves, respectively.

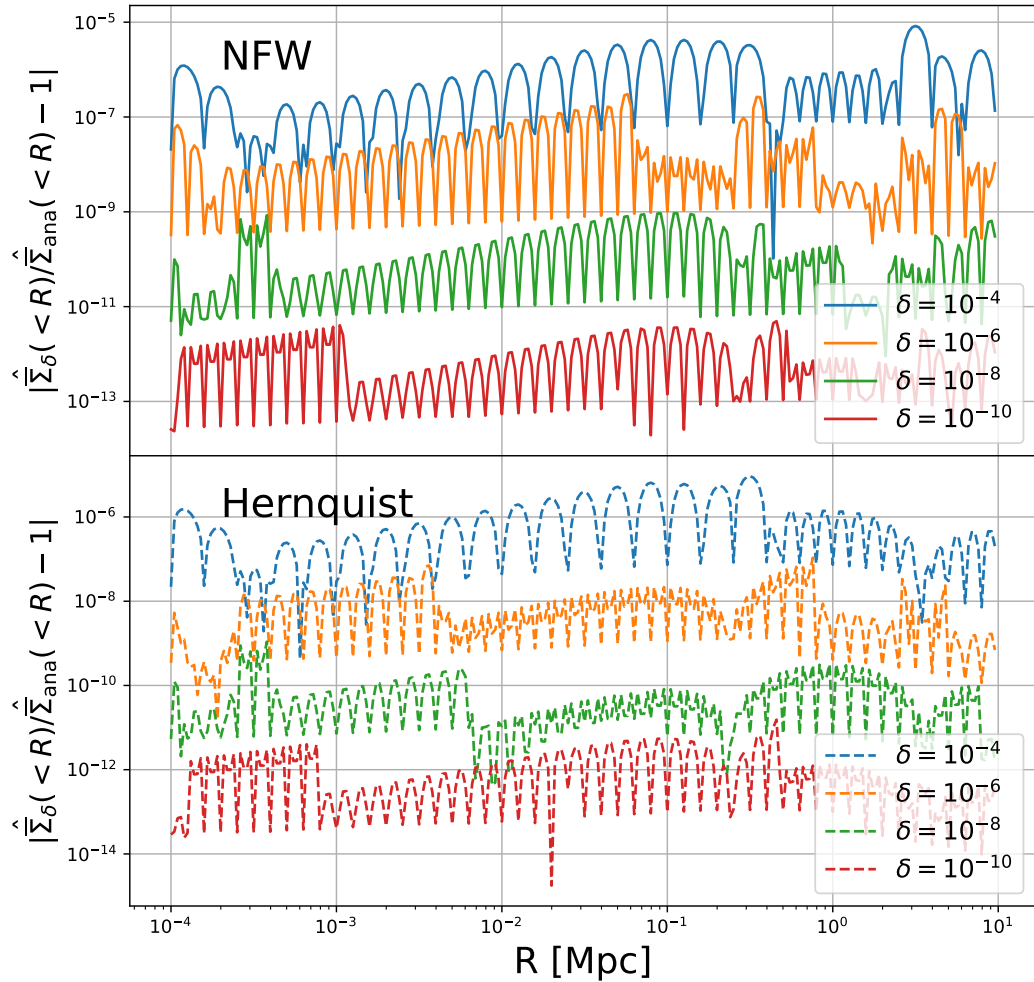


Figure 13. The relative difference between the dimensionless average surface mass density within a cylinder of radius R , $\hat{\Sigma}(\langle R \rangle)$, computed using spline interpolation and analytically for the NFW matter density profile (upper panel) and the Hernquist profile (lower panel). In both cases, the splines were built requiring a relative tolerance δ equal to 10^{-4} , 10^{-6} , 10^{-8} and 10^{-10} corresponding to the blue, orange, green and red curves, respectively.

The `refine` option, described in section 2.5, was found to be particularly useful when higher accuracy is required. Based on numerical tests, the recommended configuration is `refine = 1` and `refine_ns = 1`, as these values introduce additional knots that improve the adaptive method’s performance for more complex functions. While the impact on smooth functions was minimal, for more variable functions, it reduced the tails in the distribution of the maximum relative error, bringing the results closer to the desired tolerance. However, a drawback is that about 10% of unnecessary knots may be introduced for functions that have already met the required precision.

The analysis of the scale parameter, ε , in Section 3.3 reveals that its determination is strongly influenced by the characteristics of the function, particularly its maximum absolute value. This was demonstrated by applying $\varepsilon = 1$ to the functions $\ln(x)$ and $I_d(x)$ from section 3.1 and section 3.2, respectively. For $\ln(x)$, the effect on the approximation was minimal compared to $\varepsilon = 0$, but for $I_d(x)$, a significant improvement was observed, with a 40% reduction in the number of generated knots while maintaining nearly identical precision. This behavior is consistent not only with our method but also with other numerical techniques, including quadrature evaluations.

Interpolation-based methods for function approximation often depend on hard-coded node lists. In this work, we address this challenge with an automatic approach driven by the desired numerical precision. We present our adaptive method and algorithm, detailing the convergence criteria for knot placement and the user-defined parameters that control precision: relative tolerance, scale parameter, `refine` option, and `refine_ns` parameter.

We then demonstrate the application of this method in NumCosmo, using it to calculate the surface mass density (and its average) for NFW and Hernquist density profiles. The results show that the relative tolerance is typically about one order of magnitude larger than the desired precision.

As numerical calculations in cosmology and astrophysics become more complex and computationally expensive, the use of interpolation methods has become widespread. Many existing codes rely on hard-coded node lists, with tests conducted for only a small set of examples. However, in statistical analyses performed over multi-dimensional parameter spaces, there is often no control over the numerical precision of these calculations. This method offers a solution, ensuring analyses are both optimized and efficient while meeting the required precision.

Acknowledgments

SDPV acknowledges the support of CNPq of Brazil under grant PQ-II 316734/2021-7.

References

- [1] M. Levi, L.E. Allen, A. Raichoor, C. Baltay, S. BenZvi, F. Beutler et al., *The Dark Energy Spectroscopic Instrument (DESI)*, in *Bulletin of the American Astronomical Society*, vol. 51, p. 57, Sept., 2019, DOI [1907.10688].
- [2] N. Benitez, R. Dupke, M. Moles, L. Sodre, J. Cenarro, A. Marin-Franch et al., *J-PAS: The Javalambre-Physics of the Accelerated Universe Astrophysical Survey*, *arXiv e-prints* (2014) arXiv:1403.5237 [1403.5237].
- [3] Euclid Collaboration, Y. Mellier, Abdurro’uf, J.A. Acevedo Barroso, A. Achúcarro, J. Adamek et al., *Euclid. I. Overview of the Euclid mission*, *arXiv e-prints* (2024) arXiv:2405.13491 [2405.13491].

- [4] LSST Dark Energy Science Collaboration, *Large Synoptic Survey Telescope: Dark Energy Science Collaboration*, *arXiv e-prints* (2012) arXiv:1211.0310 [1211.0310].
- [5] O. Dore, C. Hirata, Y. Wang, D. Weinberg, T. Eifler, R.J. Foley et al., *WFIRST: The Essential Cosmology Space Observatory for the Coming Decade*, *BAAS* **51** (2019) 341 [1904.01174].
- [6] E. Di Valentino, O. Mena, S. Pan, L. Visinelli, W. Yang, A. Melchiorri et al., *In the realm of the Hubble tension—a review of solutions*, *Classical and Quantum Gravity* **38** (2021) 153001 [2103.01183].
- [7] M. Kamionkowski and A.G. Riess, *The Hubble Tension and Early Dark Energy*, *Annual Review of Nuclear and Particle Science* **73** (2023) 153 [2211.04492].
- [8] A.G. Riess and L. Breuval, *The Local Value of H_0* , in *IAU Symposium*, R. de Grijs, P.A. Whitelock and M. Catelan, eds., vol. 376 of *IAU Symposium*, pp. 15–29, Jan., 2024, DOI [2308.10954].
- [9] A. Lewis and A. Challinor, “CAMB: Code for Anisotropies in the Microwave Background.” Astrophysics Source Code Library, record ascl:1102.026, Feb., 2011.
- [10] J. Lesgourgues, *The Cosmic Linear Anisotropy Solving System (CLASS) I: Overview*, *arXiv e-prints* (2011) arXiv:1104.2932 [1104.2932].
- [11] B. Diemer, *COLOSSUS: A Python Toolkit for Cosmology, Large-scale Structure, and Dark Matter Halos*, *The Astrophysical Journal Supplement Series* **239** (2018) 35 [1712.04512].
- [12] N.E. Chisari, D. Alonso, E. Krause, C.D. Leonard, P. Bull, J. Neveu et al., *Core Cosmology Library: Precision Cosmological Predictions for LSST*, *The Astrophysical Journal Supplement Series* **242** (2019) 2 [1812.05995].
- [13] S. Dias Pinto Vitenti and M. Penna-Lima, “NumCosmo: Numerical Cosmology.” Astrophysics Source Code Library, record ascl:1408.013, Aug., 2014.
- [14] M.J.D. Powell, *Approximation Theory and Methods*, Cambridge University Press (1981).
- [15] D. Obradovic, L.N. Mishra and V.N. Mishra, *Interpolation and Approximation of Functions*, *Journal of Pure and Applied Mathematics* **5** (2021) 5 .
- [16] J. Quiñonero-Candela, C.E. Rasmussen and C.K.I. Williams, *Approximation Methods for Gaussian Process Regression*, in *Large-Scale Kernel Machines*, The MIT Press (2007), DOI [https://direct.mit.edu/book/chapter-pdf/2286468/9780262255790_cai.pdf].
- [17] N. Quadrianto, K. Kersting and Z. Xu, *Gaussian process*, in *Encyclopedia of Machine Learning*, (Boston, MA), pp. 428–439, Springer US (2010), DOI.
- [18] T. Lyche and K. Mørken, *The sensitivity of a spline function to perturbations of the knots*, *BIT Numerical Mathematics* **39** (1999) 305.
- [19] D. Michel and A. Zidna, *A new deterministic heuristic knots placement for b-spline approximation*, *Mathematics and Computers in Simulation* **186** (2021) 91.
- [20] V. Goepp, O. Bouaziz and G. Nuel, *Spline regression with automatic knot selection*, *arXiv preprint arXiv:1808.01770* (2018) .
- [21] W. Li, S. Xu, G. Zhao and L.P. Goh, *Adaptive knot placement in b-spline curve approximation*, *Computer-Aided Design* **37** (2005) 791.
- [22] R. Goldenthal and M. Bercovier, *Spline curve approximation and design by optimal control over the knots*, in *Geometric Modelling*, pp. 53–64, Springer (2004).
- [23] A. Gálvez, A. Iglesias, A. Avila, C. Otero, R. Arias and C. Manchado, *Elitist clonal selection algorithm for optimal choice of free knots in b-spline data fitting*, *Applied Soft Computing* **26** (2015) 90.

- [24] H. Idais, M. Yasin, M. Pasadas and P. González, *Optimal knots allocation in the cubic and bicubic spline interpolation problems*, *Mathematics and Computers in Simulation* **164** (2019) 131.
- [25] C. de Boor, *Convergence of cubic spline interpolation with the not-a-knot condition*, Tech. Rep. 2876, Mathematics Research Center, University of Wisconsin, 610 Walnut St. Madison WI 53705 (Oct., 1985).
- [26] P. Davis, P. Rabinowitz and W. Rheinboldt, *Methods of Numerical Integration*, Computer Science and Applied Mathematics, Elsevier Science (2014).
- [27] L.N. Trefethen, *Approximation Theory and Approximation Practice*, Society for Industrial and Applied Mathematics (2013).
- [28] C. de Boor, *A Practical Guide to Spline*, vol. 27 of *Applied Mathematical Sciences*, Springer (01, 1978), [10.2307/2006241](https://doi.org/10.2307/2006241).
- [29] M. Sun, L. Lan, C.-G. Zhu and F. Lei, *Cubic spline interpolation with optimal end conditions*, *Journal of Computational and Applied Mathematics* **425** (2023) 115039.
- [30] H. Behforooz, *Approximation by integro cubic splines*, *Applied Mathematics and Computation* **175** (2006) 8.
- [31] J.E. Phythian and R. Williams, *Direct cubic spline approximation to integrals with applications in nautical*, *International Journal for Numerical Methods in Engineering* **23** (1986) 305 [<https://onlinelibrary.wiley.com/doi/pdf/10.1002/nme.1620230212>].
- [32] C. Hall, *On error bounds for spline interpolation*, *Journal of Approximation Theory* **1** (1968) 209.
- [33] N. Ujevic and A.J. Roberts, *A corrected quadrature formula and applications*, *Anziam Journal* **45** (2003) 41.
- [34] C.O. Burg, *Derivative-based closed newton-cotes numerical quadrature*, *Applied Mathematics and Computation* **218** (2012) 7052.
- [35] K.M. Górski, E. Hivon, A.J. Banday, B.D. Wandelt, F.K. Hansen, M. Reinecke et al., *HEALPix: A Framework for High-Resolution Discretization and Fast Analysis of Data Distributed on the Sphere*, *ApJ* **622** (2005) 759 [[arXiv:astro-ph/0409513](https://arxiv.org/abs/astro-ph/0409513)].
- [36] S. Seager, D.D. Sasselov and D. Scott, *A New Calculation of the Recombination Epoch*, *ApJ* **523** (1999) L1 [[astro-ph/9909275](https://arxiv.org/abs/astro-ph/9909275)].
- [37] M. Aguena, C. Avestruz, C. Combet, S. Fu, R. Herbonnet, A.I. Malz et al., *CLMM: a LSST-DESC cluster weak lensing mass modeling library for cosmology*, *MNRAS* **508** (2021) 6092 [[2107.10857](https://arxiv.org/abs/2107.10857)].
- [38] J.F. Navarro, C.S. Frenk and S.D.M. White, *The Structure of Cold Dark Matter Halos*, *ApJ* **462** (1996) 563 [[astro-ph/9508025](https://arxiv.org/abs/astro-ph/9508025)].
- [39] L. Hernquist, *An Analytical Model for Spherical Galaxies and Bulges*, *ApJ* **356** (1990) 359.
- [40] G.D. Knott, *Interpolating cubic splines*, vol. 18 of *Progress in Computer Science and Applied Logic*, Springer Science & Business Media (2000).
- [41] T.-L. Tsai, J.-C. Yang and L.-H. Huang, *Characteristics method using cubic-spline interpolation for advection-diffusion equation*, *Journal of Hydraulic Engineering* **130** (2004) 580.
- [42] J. Ahlberg, J. Walsh, R. Bellman and E.N. Nilson, *The theory of splines and their applications*, Academic press (1967).
- [43] E. Angerson, Z. Bai, J. Dongarra, A. Greenbaum, A. McKenney, J. Du Croz et al., *LAPACK: A portable linear algebra library for high-performance computers*, in *Supercomputing '90: Proceedings of the 1990 ACM/IEEE Conference on Supercomputing*, pp. 2–11, 1990, [DOI](https://doi.org/10.1109/SUPER.1990.115547).

A Algorithmic Implementation

A.1 Cubic Spline Interpolation

In this appendix, we provide an overview of cubic spline interpolation, with a focus on the algorithmic implementation. The goal is to present an optimized solution to the interpolation problem by reformulating it in a linear algebraic framework.

Let $f(x)$ be a function defined over the interval $[a, b]$, with $n+1$ knots such that $a = x_0 < x_1 < \dots < x_n = b$, where $i = 0, 1, \dots, n-1$. For each consecutive pair of knots (x_i, x_{i+1}) , a third-order polynomial $P_i(x)$ is constructed, ensuring that the polynomial satisfies the conditions of continuity for both the first and second derivatives. The general form of $P_i(x)$ is:

$$P_i(x) = a_i + b_i(x - x_i) + c_i(x - x_i)^2 + d_i(x - x_i)^3, \quad (A.1)$$

$$x \in [x_i, x_{i+1}],$$

where a_i, b_i, c_i , and d_i are the coefficients to be determined. The overall cubic spline function, which interpolates $f(x)$ over the entire interval, is defined piecewise as follows:

$$P(x) = \begin{cases} P_0(x), & x \in [x_0, x_1), \\ P_1(x), & x \in [x_1, x_2), \\ \vdots \\ P_{n-1}(x), & x \in [x_{n-1}, x_n]. \end{cases} \quad (A.2)$$

This piecewise cubic polynomial is the basis of the cubic spline interpolation method, ensuring smoothness and continuity at the interior knots while matching the function values at the boundary knots.

To determine the $4n$ polynomial coefficients, we need to impose a set of conditions to ensure the uniqueness of the spline. The first set of constraints ensures that the cubic spline matches the function values at the given data points $\{x_i\}$. Specifically, for each knot x_i , the spline must satisfy:

$$P_i(x_i) = f(x_i) = a_i. \quad (A.3)$$

This gives $n+1$ linear constraints, corresponding to the function values at the knots, for $i = 0, \dots, n$. In addition to matching the function values, the spline must also be smooth at the $n-1$ interior knots. Since each interior knot x_i is shared by two adjacent polynomials $P_i(x)$ and $P_{i+1}(x)$, we require that the spline be continuous and have continuous first- and second-order derivatives at each interior knot. These continuity conditions are:

$$P_i(x_{i+1}) = P_{i+1}(x_{i+1}), \quad (A.4)$$

$$P'_i(x_{i+1}) = P'_{i+1}(x_{i+1}), \quad (A.5)$$

$$P''_i(x_{i+1}) = P''_{i+1}(x_{i+1}), \quad (A.6)$$

for $i = 0, \dots, n-2$, where P'_i and P''_i denote the first and second derivatives of $P_i(x)$, respectively. These conditions ensure that the spline is C^2 -continuous across the interval.

Next, we express these continuity conditions in terms of the polynomial coefficients. The first condition, eq. (A.4), gives:

$$a_i + b_i h_i + c_i h_i^2 + d_i h_i^3 = a_{i+1}, \quad (A.7)$$

where $h_i = x_{i+1} - x_i$. The second condition, eq. (A.5), leads to:

$$b_i + 2c_i h_i + 3d_i h_i^2 = b_{i+1}, \quad (\text{A.8})$$

and the third condition, eq. (A.6), yields:

$$c_i + 3d_i h_i = c_{i+1}. \quad (\text{A.9})$$

These equations must be satisfied for $i = 0, \dots, n-2$, while no continuity constraints are required at the last or first knot.

Thus far, we have established $4n-2$ conditions: $n+1$ from matching the function values at the knots and $3(n-1)$ from the continuity conditions at the interior knots. At this stage, the equations derived apply to any cubic spline interpolation. The two remaining conditions come from the choice of endpoint conditions. There are four possible types of endpoint conditions: first derivative, second derivative, quadratic, and not-a-knot constraints [40]. The first two require continuous first and second derivatives of the interpolated function, with results depending on derivative approximations [41]. In this work, we apply the not-a-knot condition [25, 28, 42], which is expressed as:

$$P_0'''(x_1) = P_1'''(x_1), \quad \Leftrightarrow \quad d_0 = d_1, \quad (\text{A.10})$$

$$P_{n-2}'''(x_{n-1}) = P_{n-1}'''(x_{n-1}), \quad \Leftrightarrow \quad d_{n-2} = d_{n-1}, \quad (\text{A.11})$$

where $P_i'''(x_i)$ denotes the third derivative of $P_i(x)$ evaluated at x_i . These conditions ensure that the third derivatives at the start and end of the mesh are equal, effectively treating the knots at these points as non-knot points. In our implementation, we required at least six (6) knots to apply the not-a-knot condition.

A.1.1 Formulating the Linear System for Spline Coefficients

To compute the cubic spline approximation under the knot-a-knot condition, we must solve for the coefficients a_i , b_i , c_i , and d_i in the cubic polynomial representation of each segment. The knot-a-knot condition, explained in the preceding sections, leads to a system of $4n$ linear constraints. In this section, we reformulate the problem into a matrix equation, reducing the unknowns to the c_i coefficients, which are the second derivatives at each knot.

We begin by applying eq. (A.3) to eq. (A.7) to determine the coefficients a_i and establish additional constraints involving b_i , c_i , and d_i . Substituting eq. (A.3) into eq. (A.7), we write:

$$f_i + b_i h_i + c_i h_i^2 + d_i h_i^3 = f_{i+1}, \quad (\text{A.12})$$

where $f_i = f(x_i)$. This equation holds for $i = 0, \dots, n-1$, ensuring that the spline matches the function values at the knots, including the boundary condition $P_{n-1}(x_n) = f(x_n)$.

Note that eq. (A.8) depends on the difference between the coefficients b_i of adjacent polynomials, defined as $\Delta b_i \equiv b_{i+1} - b_i$. Because of this, we cannot directly use it to solve for b_i and eliminate its dependence in eq. (A.12). Instead, we subtract eq. (A.12) for the indices $i+1$ and i , resulting in:

$$\Delta b_i = \Delta^x f_i - (c_{i+1} h_{i+1} - c_i h_i) - (d_{i+1} h_{i+1}^2 - d_i h_i^2), \quad (\text{A.13})$$

$$\Delta f_i \equiv f_{i+1} - f_i, \quad (\text{A.14})$$

$$\Delta^x f_i \equiv \frac{\Delta f_{i+1}}{h_{i+1}} - \frac{\Delta f_i}{h_i}. \quad (\text{A.15})$$

Here, eq. (A.13) establishes a connection between the coefficients of consecutive polynomials. It is valid for $i = 0, \dots, n-2$, as eq. (A.8) is not defined at $i = n-1$. Substituting eq. (A.8) into eq. (A.13) gives:

$$c_{i+1}h_{i+1} + c_i h_i = \Delta^x f_i - (d_{i+1}h_{i+1}^2 + 2d_i h_i^2). \quad (\text{A.16})$$

However, eq. (A.16) still depends on the coefficients d_i and d_{i+1} , which are unknown. To eliminate these variables, we use eq. (A.9) to express d_i in terms of c_i and c_{i+1} . The challenge is that eq. (A.9) is not defined at $i = n-1$. To address this, we introduce a new variable c_n and extend eq. (A.9) with an additional constraint:

$$c_{n-1} + 3d_{n-1}h_{n-1} = c_n. \quad (\text{A.17})$$

This extension allows us to express d_i in terms of c_i and c_{i+1} for all $i = 0, \dots, n-1$:

$$d_i = \frac{1}{3} \frac{c_{i+1} - c_i}{h_i}. \quad (\text{A.18})$$

Substituting eq. (A.18) into eq. (A.16), we eliminate d_i and express the system purely in terms of the c_i coefficients:

$$\frac{h_{i+1}}{3} c_{i+2} + \frac{2}{3} (h_i + h_{i+1}) c_{i+1} + \frac{h_i}{3} c_i = \Delta^x f_i, \quad (\text{A.19})$$

valid for $i = 0, \dots, n-2$. This completes the formulation of the system of equations for the c_i coefficients.

This is a good point to summarize the current state of the problem. We have reduced the interpolation task to solving for the $n+1$ coefficients c_i in the system of linear equations defined by eq. (A.19). Once the c_i coefficients are determined, the remaining coefficients a_i , b_i , and d_i can be computed using eqs. (A.3), (A.12), and (A.18), respectively. However, the system is currently underdetermined, as it consists of $n-1$ equations for $n+1$ unknowns. To address this, we introduce additional constraints. The not-a-knot condition, specified by eqs. (A.10) and (A.11), provides the two additional equations required to determine the system fully.

The challenge lies in the fact that the not-a-knot condition (or other endpoint conditions) often imposes constraints on the coefficients c_i , which can render the system singular. To address this, the system must be reformulated to ensure the coefficients c_i are uniquely determined. However, depending on how the system is constructed, the tri-diagonal structure of the matrix—crucial for computational efficiency—may be lost. To maintain both well-posedness and computational tractability, the coefficient matrix must be carefully constructed to preserve its tri-diagonal structure.

This is achieved by initially solving for c_0 , c_1 , c_{n-1} , and c_n . The not-a-knot conditions given in eqs. (A.10) and (A.11) are applied to eq. (A.18), resulting in the following equations:

$$\frac{c_1 - c_0}{h_0} = \frac{c_2 - c_1}{h_1}, \quad (\text{A.20})$$

$$\frac{c_{n-1} - c_{n-2}}{h_{n-2}} = \frac{c_n - c_{n-1}}{h_{n-1}}. \quad (\text{A.21})$$

Solving for c_0 in eq. (A.20) yields:

$$c_0 = \frac{(h_0 + h_1)c_1 - h_0 c_2}{h_1}. \quad (\text{A.22})$$

Substituting c_0 into eq. (A.19) for $i = 0$ gives an expression for c_1 :

$$c_1 = \frac{3h_1\Delta^x f_0 + (h_0^2 - h_1^2) c_2}{(h_0 + h_1)(h_0 + 2h_1)}. \quad (\text{A.23})$$

Applying this result to eq. (A.19) for $i = 1$ leads to:

$$\left(\frac{2}{3}(h_1 + h_2) + \frac{\beta h_1}{3}\right) c_2 + \frac{h_2}{3} c_3 = -\alpha\Delta^x f_0 + \Delta^x f_1, \quad (\text{A.24})$$

where:

$$\beta \equiv \frac{h_0 - h_1}{h_0 + 2h_1}, \quad (\text{A.25})$$

$$\alpha \equiv \frac{h_1^2}{(h_0 + h_1)(h_0 + 2h_1)}. \quad (\text{A.26})$$

Similarly, for $i = n - 2$, we solve for c_n and c_{n-1} :

$$c_n = \frac{(h_{n-2} + h_{n-1})c_{n-1} - h_{n-1}c_{n-2}}{h_{n-2}}, \quad (\text{A.27})$$

$$c_{n-1} = \frac{3h_{n-1}\Delta^x f_{n-2} + (h_{n-1}^2 - h_{n-2}^2) c_{n-2}}{(h_{n-2} + h_{n-1})(2h_{n-2} + h_{n-1})}. \quad (\text{A.28})$$

For c_{n-2} , the following equation is obtained:

$$\left(\frac{2}{3}(h_{n-3} + h_{n-2}) + \frac{\gamma h_{n-2}}{3}\right) c_{n-2} + \frac{h_{n-3}}{3} c_{n-3} = \Delta^x f_{n-3} - \eta\Delta^x f_{n-2}, \quad (\text{A.29})$$

where:

$$\gamma \equiv \frac{h_{n-1} - h_{n-2}}{h_{n-1} + 2h_{n-2}}, \quad (\text{A.30})$$

$$\eta \equiv \frac{h_{n-2}^2}{(h_{n-2} + h_{n-1})(2h_{n-2} + h_{n-1})}. \quad (\text{A.31})$$

Finally, with the updated relations for these coefficients, the tri-diagonal matrix defined by eq. (A.19) for $i = 2, \dots, n - 2$ is represented by T :

$$T \equiv \begin{bmatrix} (2 + \beta)h_1 + 2h_2 & h_2 & 0 & \dots & \dots & 0 \\ h_2 & 2(h_2 + h_3) & h_3 & 0 & \dots & \vdots \\ 0 & h_3 & 2(h_3 + h_4) & h_4 & 0 & \vdots \\ \vdots & 0 & \ddots & \ddots & \ddots & 0 \\ 0 & \vdots & 0 & h_{n-4} & 2(h_{n-4} + h_{n-3}) & h_{n-3} \\ 0 & 0 & \dots & 0 & h_{n-3} & 2h_{n-3} + (2 + \gamma)h_{n-2} \end{bmatrix}, \quad (\text{A.32})$$

which is a symmetric positive-definite tri-diagonal matrix. The full system of equations is then given by:

$$T \times \begin{bmatrix} c_2 \\ c_3 \\ \vdots \\ \vdots \\ \vdots \\ c_{n-3} \\ c_{n-2} \end{bmatrix} = 3 \begin{bmatrix} -\alpha \Delta^x f_0 + \Delta^x f_1 \\ \Delta^x f_2 \\ \vdots \\ \vdots \\ \vdots \\ \Delta^x f_{n-4} \\ \Delta^x f_{n-3} - \eta \Delta^x f_{n-2} \end{bmatrix}. \quad (\text{A.33})$$

This problem is reduced to solving a tri-diagonal system of equations, a computationally efficient task due to the sparse structure of the coefficient matrix. Since the matrix is symmetric, we use the LAPACK library [43], specifically the routine `dptsv`, which is optimized for solving symmetric positive-definite tri-diagonal systems. This routine computes the solution for the coefficients c_2, \dots, c_{n-2} , ensuring numerical stability and efficiency.

Once these intermediate coefficients are determined, the remaining boundary coefficients c_0, c_1, c_{n-1} , and c_n are computed using eqs. (A.22), (A.23), (A.27), and (A.28). With all coefficients c_i now established, the polynomial coefficients a_i, b_i , and d_i for each interval are obtained by substituting the results into eqs. (A.3), (A.12), and (A.18), respectively. This sequential computation ensures that the cubic spline interpolation is fully defined, preserving continuity and smoothness across all sub-intervals while imposing to the not-a-knot boundary conditions.

A.2 Adaptive Spline Function

The `ncm_spline_func` algorithm constructs an adaptive spline representation of a function $f(x)$ by iteratively refining intervals to meet specified error tolerances. A linked list is employed as the primary data structure, enabling efficient insertion of new points during the adaptive process. The algorithm starts with an initial set of points and evaluates the midpoint \bar{x}_i for each interval. It then checks error criteria based on absolute and integral estimates (2.8). If the adaptive criteria are not satisfied ($s_i < s_{\text{conv}}$), the interval is subdivided, and \bar{x}_i is inserted into the list, ensuring that each function evaluation contributes to improving the spline.

When no further refinement is detected, a secondary step is triggered to address intervals with large segment lengths. This step resets intervals exceeding a threshold based on the standard deviation of segment lengths for further refinement. By combining adaptive and statistical criteria, the AutoKnots algorithm efficiently constructs a robust spline representation that balances accuracy and computational cost, particularly in regions where higher resolution is required.

Algorithm 1 ncm_spline_func

```
 $\delta \leftarrow [2.22045 \times 10^{-16}, 1]$  ▷ (default:  $10^{-8}$ )  
 $\varepsilon \leftarrow [0, \infty)$  ▷ (default: 0)  
 $s_{\text{conv}} \leftarrow \mathbb{Z}^+$  ▷ (default: 1)  
refine  $\leftarrow \mathbb{Z}^{0+}$  ▷ (default: 1)  
refine_ns  $\leftarrow (0, \infty)$  ▷ (default: 1)  
 $t \leftarrow 0$   
 $\mathbb{K}^t \leftarrow \{(x_i, f(x_i), s_i = 0)\}_{m=6}$  ▷ linked list  
improve  $\leftarrow \text{True}$   
while improve do ▷ cubic-spline-notaknot  
   $\hat{f}^t \leftarrow \text{interpolate}(\mathbb{K}^t)$   
   $\mathbb{K}^{t+1} \leftarrow \mathbb{K}^t$   
  improve  $\leftarrow \text{False}$   
  for  $i \leftarrow 0$  to  $\text{len}(\mathbb{K}^t) - 2$  do ▷ midpoint-rule  
     $\bar{x}_i \leftarrow \frac{x_i + x_{i+1}}{2}$   
    if  $s_i < s_{\text{conv}}$  then  
       $\bar{f} \leftarrow f(\bar{x}_i)$   
       $h_i \leftarrow x_{i+1} - x_i$   
       $\Delta^a f \leftarrow \left| \bar{f} - \hat{f}^t(\bar{x}_i) \right|$   
       $\hat{\mathcal{I}} \leftarrow \text{integral}(\hat{f}^t, x_i, x_{i+1})$   
       $\tilde{\mathcal{I}} \leftarrow \text{simpson}(x_i, \bar{x}_i, x_{i+1})$   
       $\Delta \mathcal{I} \leftarrow \left| \hat{\mathcal{I}} - \tilde{\mathcal{I}} \right|$   
      if  $\Delta^a f \leq \delta (|\bar{f}| + \varepsilon)$  and  $\Delta \mathcal{I} \leq \delta (|\tilde{\mathcal{I}}| + \varepsilon h_i)$  then  
         $s_i \leftarrow s_i + 1$   
      else  
        improve  $\leftarrow \text{True}$   
      end if  
       $\mathbb{K}^{t+1} \leftarrow \mathbb{K}^{t+1} \cup \{(\bar{x}_i, \bar{f}, s_i)\}$  ▷ insert-after  $i$   
    end if  
  end for  
if not improve and refine  $> 0$  then  
   $\mathbb{H}^t \leftarrow \{h_i\}$   
  refine  $\leftarrow \text{refine} - 1$   
   $\mu \leftarrow \text{mean}(\mathbb{H}^t)$   
   $\sigma \leftarrow \text{std}(\mathbb{H}^t)$   
  for  $i \leftarrow 0$  to  $\text{len}(\mathbb{K}^t) - 2$  do  
    if  $h_i > \text{refine\_ns} \cdot \sigma$  then  
       $s_i \leftarrow 0$   
      improve  $\leftarrow \text{True}$   
    end if  
  end for  
end if  
end while  
return  $\mathbb{K}^t$ 
```
